# Solid Acidic Catalysts for the Production of Bio-substitutes for Petrochemical Intermediates

Qun Zhao

A Thesis

in

The Department

of

Chemistry and Biochemistry

Presented in Partial Fulfillment of the Requirements
For the Degree of Master of Science at
Concordia University
Montreal, Quebec, Canada

October 2007

*Your file Votre référence*
*ISBN: 978-0-494-40859-9*
*Our file Notre référence*
*ISBN: 978-0-494-40859-9*

## Abstract

Solid Acidic Catalysts for the Production of Bio-substitutes for Petrochemical Intermediates

Qun Zhao, M. Sc.

Light olefins such as ethylene and propylene are the most important chemical monomers used for the production of plastics and synthetic fibres. They are usually obtained by cracking (steam cracking or fluid catalytic cracking) of hydrocarbons from petroleum gas oils, and are generally called petrochemical intermediates. As we know, ethylene can also be produced through dehydration of ethanol obtained by fermentation of biomass materials (bioethanol). This may be an alternative way for obtaining the petrochemical intermediates.

In the present work, catalytic dehydration of aqueous ethanol (ethanol in aqueous solution) over some solid acidic catalysts, such as dealuminated zeolite X(also called silica nanoboxes), silica nanoboxes acidified by incorporation of triflic acid, zeolite Y, zeolite USY (Ultra Stable zeolite Y), zeolite ZSM-5 etc. (all in acidic form) has been studied. Dealuminated zeolite X has been obtained by AHFS (ammonium hexafluorosilicate) dealumination technique and has been fully characterized. Influences of experimental conditions on the textural properties of the porous products in dealumination of NaA, NaX, $NH_4Y$ zeolites and Na mordenite by AHFS treatment have been investigated. It has been found that the decreasing order of the resistance to AHFS dealuminating action is as follows: Na mordenite > $NH_4Y$ zeolites > NaX zeolite > NaA zeolite; and only NaA and NaX zeolites can be used as starting materials for preparation

of mesoporous aluminosilicates by pore enlargement technique of AHFS dealumination. Mesoporous materials obtained from X zeolite(also called silica nanoboxes) show a high hydrothermal stability and a quite interesting ion-exchange capacity.

Zeolite ZSM-5/50 ($SiO_2/Al_2O_3$ ratio is 50) shows the highest catalytic activity mostly when compared to the faujasite type zeolites. The order of catalytic activity for the catalysts is explained by their surface acidity (density and strength). Therefore, the second part of this study was based on the zeolite ZSM-5. For the ZSM-5 series, an increase of $SiO_2/Al_2O_3$ ratio leads to the decrease in catalytic activity because of a decrease in their surface acidity.

The effects of reaction temperature, the WHSV (weight hourly space velocity) and the concentration of ethanol in water on the total conversion of bioethanol and on selectivity to ethylene and propylene over zeolite ZSM-5/50 are also investigated. It has been found that with increasing reaction temperature, total conversion of bioethanol increases, and nearly reaches 100% at 250°C. In temperature range of 200 - 250°C, the main product is ethylene. When the reaction temperature is higher than 250°C, the selectivity to other light olefins such as propylene and BTX aromatics significantly increases due to the further conversion of ethylene on strong acid sites. At 275°C, the yield of ethylene plus propylene reaches a maximum value.

The results also show that the yield of ethylene decreases when the WHSV increases and the yield of ethylene slightly increases when the concentration of ethanol in water increases.

## Acknowledgments

During the time of my study, many people helped me, and now I would like to take this opportunity to express my gratitude to these people.

First I would like to express my sincere thanks to my research supervisor Dr. Raymond Le Van Mao for giving me this wonderful opportunity to study in his group. His offer allowed me a chance to further develop my knowledge and skills in chemistry. His great passion of chemistry and insightful thoughts of science and technology impressed me a lot. His brilliant advice and helpful discussions guided me through my M. Sc. research.

I would also like to thank Dr. M. Judith Kornblatt and Dr. Louis A. Cuccia for being the members of my research committee and for taking time to evaluate this project. I look forward to your comments and suggestions.

I want to thank my colleague Mr. Nabil Al-Yassir. His contribution to this laboratory is tremendous. I cannot forget the time he spent on experimental set-up and instrumental troubleshooting for us. My thanks also go to current and past members of Dr. Le Van Mao's group: Ms Lin Lu, for a lot of useful discussions and friendship; Dr. Ngoc Thanh Vu, Mr. Hao Peng and Mr. Haitao Yan, for their assistance, advice and enjoyable time in laboratory.

Finally, I want to thank my husband and my lovely daughter. They have been so patient and supportive to accompany me through this long journey. Without their support, this work could not have been completed.

*Dedication*

*For my father Professor G. Zhao and my mother Professor Y. Zou*

*Without them I could never make this far in my life*

# Table of Contents

# List of Figures

Chapter 1



Chapter 3

# List of Tables

# List of Abbreviations

| | |
|---|---|
| AHFS | Ammonium Hexafluorosilicate |
| BAS | Brønsted Acid Site |
| BET | Brunauer, Emmett and Teller |
| BJH | Barrett, Joyner and Halenda |
| BTX | Benzene, Toluene and Xylene |
| CEC | Cation Exchange Capacity |
| $D_{av.}$ | Average Diameter |
| DEE | Di-ethyl Ether |
| DeX | Dealuminated Zeolite X |
| DSC | Differential Scanning Calorimetry |
| DTA/TGA | Differential Thermal Analysis/Thermogravimetric Analysis |
| EPA | Electronmicroprobe Analysis |
| ETH | Ethanol to Hydrocarbon |
| FCC | Fluid Catalytic Cracking |
| IEC | Ion-exchange Capacity |
| ISE | Ion-selective Electrode |
| LAS | Lewis Acid Site |
| LZY-82 | $NH_4Y$ Zeolite |
| MAS NMR | Magic-Angle Spinning Nuclear Magnetic Resonance |
| MCF | Mesocellular Foam |
| MCM-41 | Mobile Crystalline Material |

| | |
|---|---|
| MIP | Mercury Intrusion Porosimetry |
| $NH_3$-TPD | Ammonia Temperature Program Desorption |
| $S_{BET}$ | BET Surface Area |
| TFA | Trifloromethanesulfonic Acid |
| USY | Ultra Stable Zeolite Y |
| $V_{mic}$ | Volume of Micropore |
| $V_t$ | Total Volume |
| WHSV | Weight Hourly Space Velocity |
| XRD | X-ray Powder Diffraction |
| XRF | X-ray Fluorescence |
| ZSM | Zeolite Socony Mobil |

# Chapter 1 Introduction and Literature Review

## 1.1 Introduction

Ethanol from biomass fermentation is considered as an interesting intermediate for chemicals and solvents because it is not derived from petroleum, is at least neutral in terms of greenhouse gas emission ($CO_2$), and is a renewable resource. However, the aqueous ethanol from fermentation of sugars (most likely glucose) should maintain a concentration range of 20 wt% to 25 wt% in order to keep those enzymes active. A subsequent distillation step is necessary to obtain the 95% ethanol and a further drying step is needed for obtaining absolute ethanol. Distillation is a high energy consuming step, and thus the production cost of ethylene obtained by catalytic dehydration using 95% or absolute ethanol from biomass is still more expensive when comparing to the use of low cost petroleum ethanol. Therefore, the use of aqueous ethanol(aqueous solution of ethanol 20-25 wt%) to catalytically produce ethylene and other light olefins such as propylene can be seen as a move towards a decrease of the production cost of those olefinic products, the distillation step of ethanol being combined with its conversion to hydrocarbons. However, the large amount of water in aqueous ethanol (specifically 20 wt% or 25 wt% ethanol) should not negatively affect the properties of the conversion catalyst or the efficiency of energy recovery during the phase of product cooling. In the present work, 20 wt% ethanol water solution is used to simulate bio-ethanol directly from fermentation broth.

Zeolites appear to be the most suitable catalysts for the production of ethylene from aqueous ethanol[1-4]. These crystalline materials are also resistant to the effect of water (steam), at least at relatively low reaction temperature.

In recent times, the reduction of $CO_2$ emission has become a crucial problem in the chemical industry. The utilization of substitutes for petrochemical intermediates from biomass becomes more interesting, especially conversion of ethanol obtained by biomass fermentation may facilitate the reduction of $CO_2$ emission. Therefore, many researchers have focused attention on the catalytic conversion of ethanol. Figure 1.1 shows the future of substitutes for petrochemical intermediates from biomass.

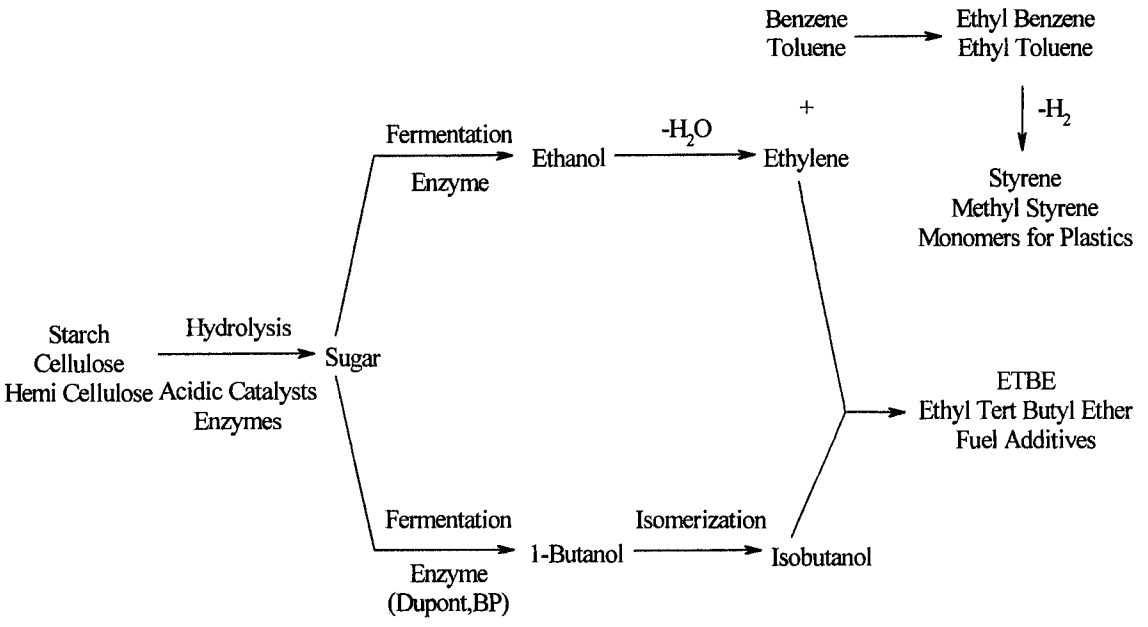


Figure 1.1 Future of substitutes for petrochemical intermediates from biomass

## 1.2 A Brief Summary on Ethanol Dehydration

Ethylene is one of the most important chemical and intermediate in the petrochemical industry. It can be obtained by the cracking of hydrocarbons from oil or by the dehydration of ethanol from fermentation of sugar. Early in the 1980s, some studies were made on catalytic dehydration of ethanol to ethylene[3-6] using solid acids such as alumina or zeolites as catalysts. Several related processes were reported in patents[7, 8]. In Process Economics Program (PEP) Review[9], process designs and economic estimates were presented for fixed-bed and fluidized-bed processes for catalytic dehydration of ethanol to produce ethylene. The authors pointed out that the designs were based on production of 60,000 metric tons/yr of 99.95% ethylene from a 95 wt% ethanol feed. The fluidized-bed process appears to require a lower investment and to have a lower operating cost. Also it gives a better yield of ethylene on feed. Neither process appears capable of producing ethylene at a price competitive with that of ethylene from world-scale hydrocarbon cracking plants. However, ethanol dehydration could be of interest for relatively small-scale production in an area where public policy encouraged the development of a chemical industry based on local agricultural sources.

## 1.3 Catalysts Used in Ethanol Dehydration

In literature, several kinds of acidic catalysts have been studied for this purpose:

1. Alumina and modified alumina

In early days, aluminum oxide[6] was applied as a catalyst for the dehydration of ethanol. Winnick[7] found that by contacting an alumina with an organic silylating agent at elevated temperature, it exhibited markedly improved dehydration activity as compared to the nonsilylated catalysts.

2. Acidic sepiolite and zeolites

In a study made by Corma et al., acidic sepiolite[5] was used as a dehydration catalyst. In 1987 Le Van Mao et al.[10] applied zeolites as catalysts for the dehydration of ethanol into ethylene. Two years later, they developed a bioethanol-to-ethylene process[4], in which ethanol present at low concentration in a fermentation broth was converted into ethylene over a solid superacid catalyst (triflic acid bound to the silica rich surface of the acidic ZSM-5 zeolite). More recently, the dehydration of ethanol into ethylene was investigated over various solid acid catalysts, such as zeolites and silica - alumina, at temperatures range from 453 - 573K under atmospheric pressure[11]. The authors considered that ethylene was produced via diethyl ether during the dehydration process. H-mordenites were found to be the most active for the dehydration in this study. In the comparison of catalysts used it was suggested that the catalyst activity could be correlated with the number of strong Brønsted acid sites in the catalyst. Further, the H-mordenite was more stable with a $SiO_2/Al_2O_3$ ratio of 90 than with a $SiO_2/Al_2O_3$ ratio of 20.

In this research work, different types of zeolites (all in acid form) were used as the catalysts for the dehydration of ethanol. The total conversion and the product selectivity were studied as well.

3. Substituted phosphoric acids and zirconium phosphite

A process developed by Pearson and Donald[8] for catalytic dehydration of ethanol was carried out in the presence of water vapour. The mixture of ethanol and water vapour was contacted with the catalyst bed containing a substituted phosphoric acid catalyst. The catalyst comprises a catalyst support having absorbed a substituted phosphoric acid in which one of the hydroxyl groups has been replaced by a hydrophobic organic group containing from 4 to 22 carbons.

In 1991 Ben-Zu Wan et al. used zirconium phosphite as an acidic catalyst[12]. The nature of acidic sites on layered zirconium phosphite has been characterized by IR spectra, thermal analysis and catalytic dehydration of ethanol. The catalytic behaviour was compared with that of α-zirconium phosphate. The reaction sequences for ether and ethylene formation were studied by analyzing the kinetic data. The Brønsted acidity of monohydrogen orthophosphate groups was considered to be the common active site on α-zirconium phosphate and the zirconium phosphite sample calcined at 673K. For the latter compound, the phosphite groups on the exterior surface were found to be oxidized to phosphate by calcination in the air. The uncalcined sample of zirconium phosphite exhibited a different catalytic behaviour. Its selectivity for diethyl ether was the highest among the catalysts studied. The dehydration activity of this compound was presumed to be due to the polar P-H bonds in the phosphite groups.

4. Halide clusters of Nb, Mo, Ta and W

Kamiguchi et al.[13] used halide clusters of Nb, Mo, Ta and W possessing an octahedral metal core as catalysts. It has been found that molecular halide clusters, $[(M_6Cl_{12})Cl_2(H_2O)_4]\cdot 4H_2O$ (M = Nb, Ta) and $(H_3O)_2[(M_6Cl_8)Cl_6]\cdot 6H_2O$ (M = Mo, W), develop catalytic activity for the dehydration of alcohols to yield olefins and ethers when they are treated at 300°C. The activity of the W cluster appears at 250°C at which temperature it changes to the poorly crystallized three-dimensional linked cluster $[W_6Cl^{i}{}_8]Cl^{a}{}_4Cl^{a\text{-}a}{}_{4/2}$, and decreases at 400°C at which temperature the crystallinity improves.

5. Potassium and silver salts of tungstophosphoric acid

Potassium and silver salts of tungstophosphoric acid with varying amounts of the cations, $K_xH_{3-x}PW_{12}O_{40}$ and $Ag_xH_{3-x}PW_{12}O_{40}$, have been prepared as pure or supported on silica using the incipient wetness method. Their catalytic properties in two reactions have been studied[14]. The vapour-phase dehydration of ethanol carried out in a conventional flow-type reactor under atmospheric pressure at temperatures varying from 398 to 773K, and the hydration of ethylene in a stainless-steel batch reactor at 478K under the pressure of 42 atm. $K_xH_{3-x}PW_{12}O_{40}$ in the range $0 < x < 2$, is composed of two phases, $H_3PW_{12}O_{40}$ and $K_2H_1PW_{12}O_{40}$; in the range $2 \leq x < 3$ the solid solution is formed. Their catalytic activity in both dehydration of ethanol and hydration of ethylene decreases with increasing x, with $K_2H_1PW_{12}O_{40}$ and $K_3PW_{12}O_{40}$ being inactive in the hydration. $Ag_xH_{3-x}PW_{12}O_{40}$ forms one phase of the solid solution in the whole composition range $0 < x < 3$. The catalytic activity in both reactions increases. It has been shown that the

catalytic activity is related to acid protons and protons generated by dissociation of water molecules coordinated by silver cations. At temperatures higher than 573K the oxidative dehydrogenation of ethanol to acetaldehyde with high yield is observed on the $Ag_xH_{3-x}PW_{12}O_{40}$ series of catalysts.

6. Transition metal oxides

Zaki[15] studied catalytic ethanol dehydration using different prepared catalysts, which include $Fe_2O_3$, $Mn_2O_3$, and calcined physical mixtures of both ferric and manganese oxides with alumina and/or silica gel. The physicochemical properties of these catalysts were investigated via X-ray powder diffraction (XRD), acidity measurement, and nitrogen adsorption/desorption at -196°C. The catalytic activity of such catalysts was tested through conversion of ethanol at 200 - 500°C using a catalytic flow system operated under atmospheric pressure. The results indicated that the dehydration reaction on the catalyst relies on surface acidity, whereas the ethylene production selectivity depends on the catalysts' chemical constituents. They further investigated the effect of thermal pretreatment on manganese material properties via XRF, DSC, XRD, MIP, and surface acidity measurements[16]. The catalytic activity toward dehydration of different alcohols, such as ethanol (in comparison with synthetic manganese catalyst), 1-propanol and 1-butanol, was also carried out in a catalytic flow type system in the presence of a hydrogen stream under atmospheric pressure with reaction temperatures ranging from 200 - 550°C and at different space velocities between 0.46 - 15.40 $h^{-1}$. The results showed an agreement between manganese calcined material and the prepared catalyst in the optimum reaction temperature required for the

dehydration of ethanol to ethylene, as well as the selectivity values. Data showed a decrease in total dehydration conversion percentage in the order as follows: ethanol > 1-propanol > 1-butanol.

## 1.4 Reactions Mechanism

### 1.4.1 Primary Reactions of Ethanol Dehydration

The reaction mechanism for catalytic dehydration of ethanol has been investigated by some authors[6, 17, 18]. It has been found that products formed in the dehydration of ethanol over solid acids were ethylene, diethyl ether, and small amount of ethane, acetaldehyde, propylene and butanes[11]. This implies that the reactions involved are rather complicated. Generally speaking, ethanol dehydration over solid catalysts containing acid sites can react via two reaction path ways[19]: intra molecular dehydration and inter molecular dehydration (See Figure 1.2).

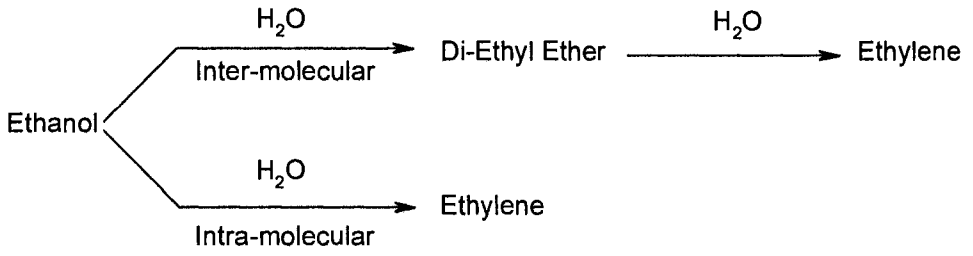


Figure 1.2 Reaction pathways of ethanol dehydration over solid catalyst

Depending on the catalyst and reaction conditions used such as reaction temperature, weight hourly space velocity (WHSV) and aqueous ethanol concentration, the product distribution may vary. The formation of diethyl ether (DEE) is favoured at low temperature and fast WHSV (low contact time), and direct formation of ethylene occurs at high temperature and slow WHSV (high contact time). It is worth mentioning that in heterogeneous catalysis, one of the key reaction parameters is the contact time($\tau$), i.e. the time during which a reaction molecule is in contact with the catalyst surface. Contact time is expressed as $\tau = W_{cat}/F_w$, where $W_{cat}$ is the catalyst weight and $F_w$ is the weight flow rate of reactant, being expressed by the weight of reactant flowing through the catalyst bed by time (h or s). Thus, the contact time is expressed in h or s. The WHSV (weight hourly space velocity), being the reciprocal of the contact time, is expressed in $h^{-1}$ or $s^{-1}$. The conversion of ethanol into ethylene occurs along pathway 2 and into diethyl ether along pathway 3. A detailed reaction mechanism is given in Figure 1.3. Ethanol first becomes adsorbed onto the Brønsted acid sites (BAS) in the vicinity of the aluminum atom and then it is followed by a rapid proton transfer from the zeolite surface forming a dihydro ethyl oxonium ion, which is highly unstable and is rapidly attacked by another ethanol molecule to form a more stable hydro diethyl oxonium ion. The rate limiting step is the formation of the ethyl (carbocation) which stabilizes itself by loss of a proton.

Chang[20,21] supported the proposal by Venuto and Landis[22] for the formation of a carbenoid species(as shown in pathway 1 in Figure1.3). After initial adsorption of the alcohol on the zeolite surface, carbenoid species are first formed and then rearrange to form ethylene.

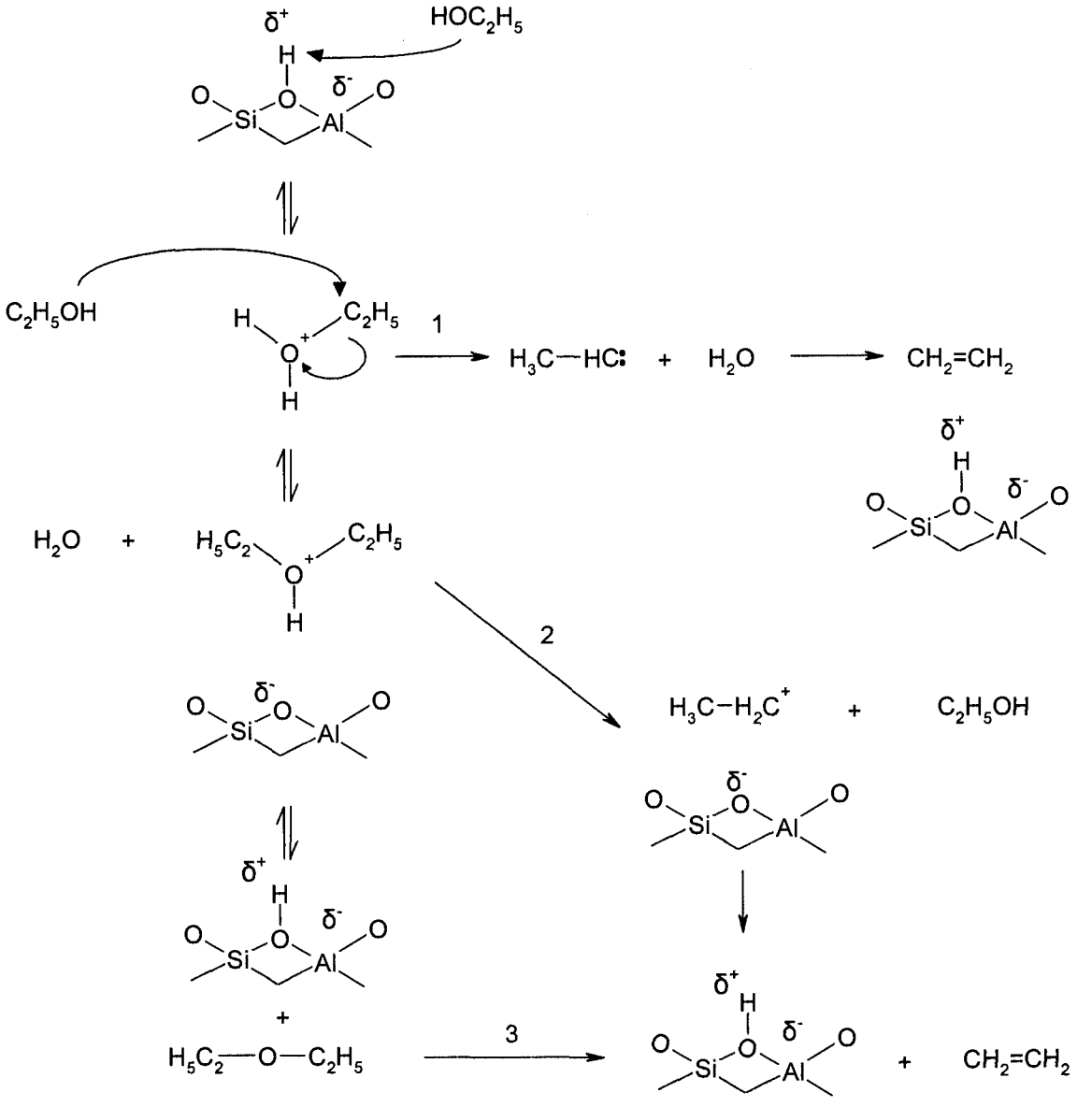


Figure 1.3 Reaction mechanism of ethanol dehydration[23]

### 1.4.2 Secondary Reactions of Ethanol Dehydration

During the dehydration of ethanol, ethylene is produced via diethyl ether; however, some other hydrocarbons can be simultaneously formed through side reactions such as: oligomerization plus cracking, metathesis and aromatization etc. As a result, the possible by-products can be methane, ethane, propylene, other $C_3$ – $C_6$ paraffins and olefins, and BTX aromatics. Different reaction conditions such as reaction temperature, aqueous ethanol concentration and WHSV (or expressed as contact time) will lead to a different total conversion. Consequently, the product selectivity of ethanol will be different as well.

1. Oligomerization

The addition of one olefin molecule to a second and to a third, etc. to form a dimer or trimer, etc. is termed oligomerization. The reaction is normally acid-catalyzed. It has been reported that oligomerization of ethylene using a Ziegler catalyst produces unbranched alpha olefins in the C12-C16 range by an insertion mechanism[24].

The oligomerization reaction produces polymer and the reaction undergoes the following steps:

1. Ethylene protonation and carbocation formation


2. The reaction of carbocation with another ethylene

3. The newly formed carbocation either eliminates a proton and forms a dimer or attacks another ethylene molecule and elimines a proton, giving a trimer.

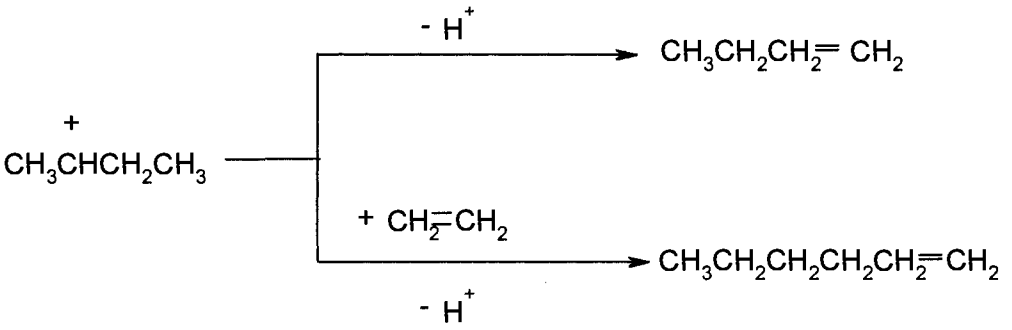


2. Catalytic Cracking

It is generally accepted the catalytic cracking of hydrocarbons occurs via a carbocation ion mechanism in the vapour phase and that the reactions can be catalyzed by any material with Brønsted or Lewis acidity[25-27]. Two reaction mechanisms are known in catalytic cracking of hydrocarbons. The first mechanism proceeds via carbenium ions, whereas the second mechanism proceeds via the formation of carbonium ions (See Figure 1.4 and 1.5).

1. Initiation step:

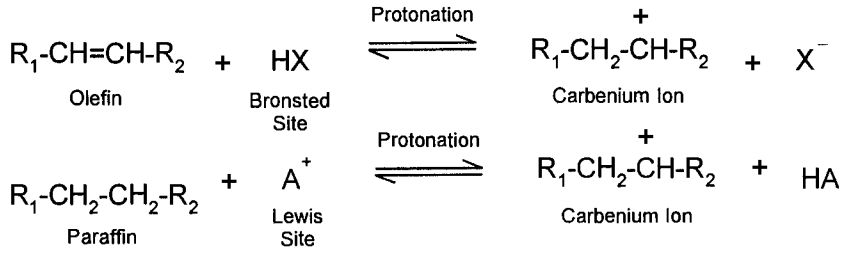


2. Propagation step (Hydride transfer):

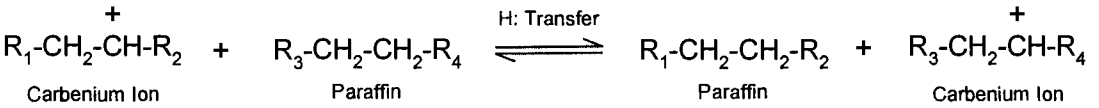


3. Cracking step (Beta-scission):

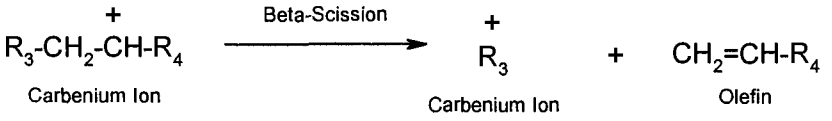


Figure 1.4 Reaction pathways involving carbenium ions[25]

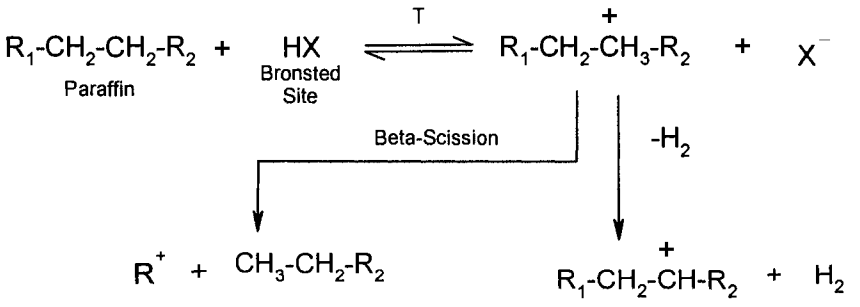


Figure 1.5 Reaction pathways involving carbonium ions[25]

3. Olefin metathesis

Yves Chauvin, Robert H. Grubbs and Richard R. Schrock developed the metathesis method[28-33] in organic synthesis and they were awarded the 2005 Nobel Prize in Chemistry. Olefin metathesis is an organic reaction which involves redistribution of alkene bonds. This reaction consists of an alkene double bond cleavage, followed by a statistical redistribution of alkylidene fragments (See Figure 1.6).

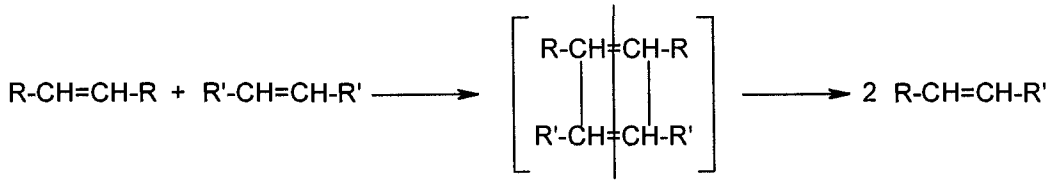


Figure 1.6 Reaction mechanism of olefin metathesis[28]

4. Aromatization

Light olefins such as ethylene and propylene can undergo oligomerization, cyclization and dehydrogenation by hydride transfer to give aromatics. A. Corma and A. Martinez have reported that aromatization occurs when the reaction is carried out on HZSM-5 at temperature about 500°C and long contact times. However, aromatization on purely acidic HZSM-5 produces large amounts of methane and ethane, thus limiting the formation of aromatics. Figure 1.7 shows reaction pathway of aromatization from olefins[34].

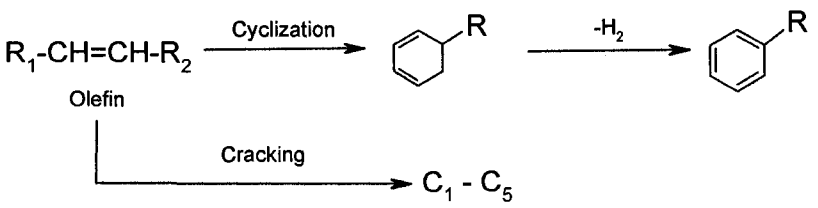


Figure 1.7 Reaction pathway of aromatization

5. "Hydrocarbon mechanism pool" hypothesis

The mechanism of methanol to olefins has been studied for a long time, there were at least 20 distinct proposals for this chemistry[35]. Dahl and Kolboe used a variety of evidence to first formulate the hydrocarbon pool mechanism for methanol conversion on HZSM-5[36,37]. The hydrocarbon pool mechanism was initially not further specified, but during the last few years, it became clear that methylbenzenes play central roles in the hydrocarbon pool mechanism. Unlike those classical mechanisms that involve oxonium-ylides, carbenium ions, carbenes, free radicals or other small energetic intermediates, hydrocarbon pool mechanism uses methylbenzene species as reaction centers for olefin production[38-41]. There are two reaction pathways to explain how methylbenzenes function as hydrocarbon pool species: the exocyclic methylation route and the paring reaction. In exocyclic methylation route, hepta-methylbenzenium cation is deprotonated into 1,2,3,3,4,5,-hexa-methyl-6-methylene-1,4-cyclohexadiene(HMMC). The exocyclic double bond then undergoes reaction with an incoming methanol molecule, resulting in an ethyl group on benzene ring, which is subsequently dealkylated as ethylene (See figure 1.8-a), also propylene formation is possible from this reaction. In the paring reaction mechanism, a benzenium cation ring contracts from six carbons to five carbons, and then expands back to six such that an alkyl chain is extended in this process. As in other hydrocarbon pool mechanism, this alkyl chain would be eliminated as an olefin (See figure 1.8-b).

A. Exocyclic methylation reaction:

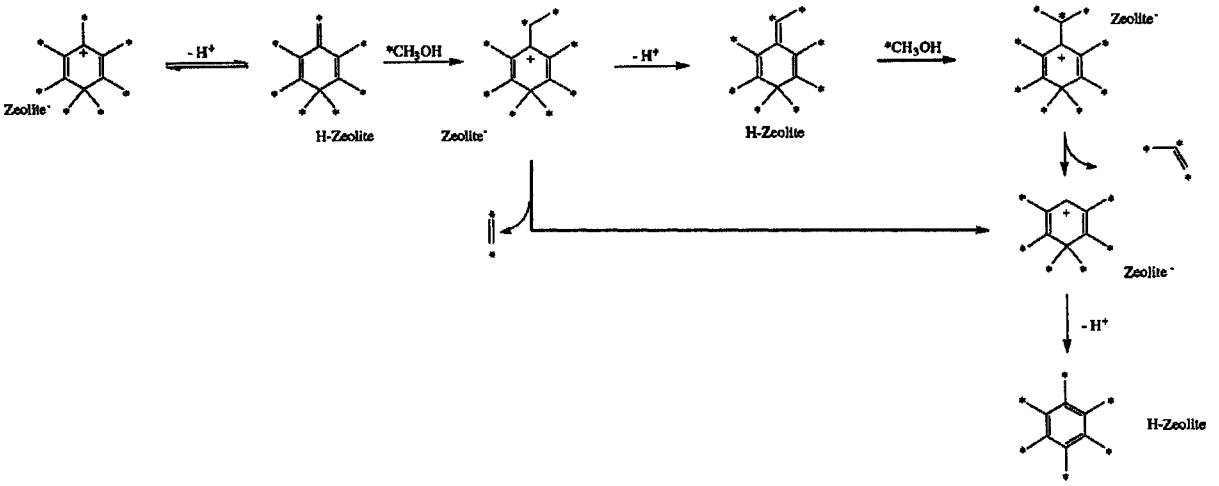


B. Paring Reaction:

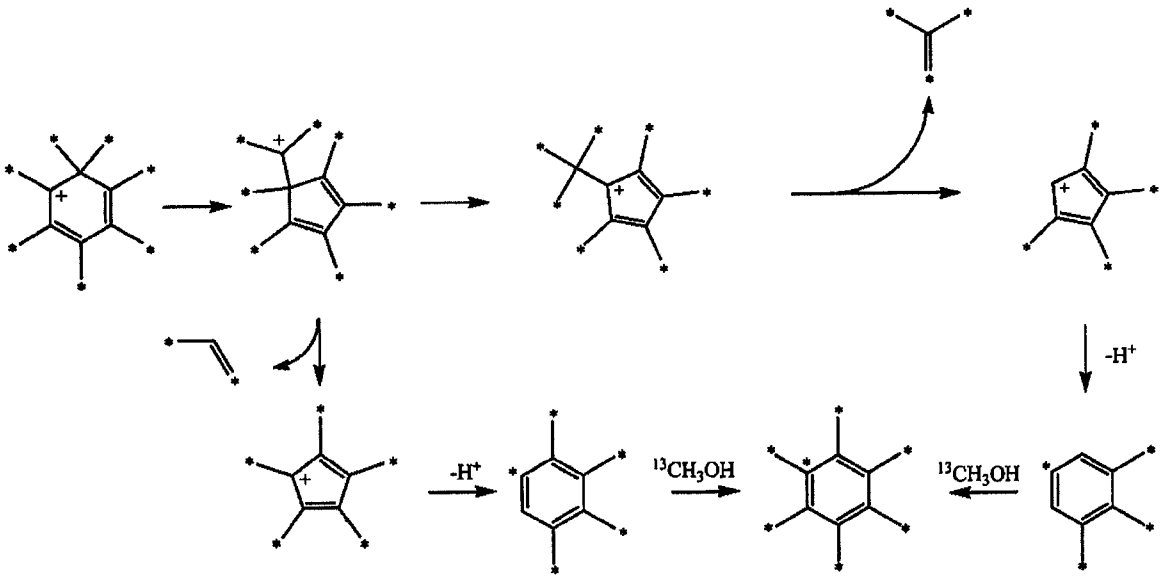


Figure 1.8 Reaction pathway of hydrocarbon pool mechanism[38]

## 1.5 Introduction to Zeolites

### 1.5.1 Zeolites and Their Characterization

Zeolites are aluminosilicate crystalline and highly porous materials, with the chemical formula of $Me_x[(AlO_2)_x(SiO_2)_y] \cdot zH_2O$, where x and y are varied depending on what type it is. Different types of zeolites will have different Si/Al ratio. Many types of zeolites are commercially available, and their chemical and physical properties are well determined (See Table 1.1). The information about their synthesis and characteristics can be easily acquired from the related books and review articles[42-45]. In the following, several types of zeolites, some of which may be selected as the starting materials for preparation of silica nanoboxes or as the catalyst in this work, will be introduced.

Table 1.1 Physical and chemical properties of zeolites[46]

| unit-cell compn | cation-exch capacity/mequiv/g: anhydrous Z | cation-exch capacity/mequiv/g: hydrated Z | Si/Al | unit-cell vol/nm$^3$ | void vol/cm$^3$/cm$^3$ | kinetic diam[a]/nm | T[b],°C |
|---|---|---|---|---|---|---|---|
| $Na_{12}[(AlO_2)_{12}(SiO_2)_{12}]\cdot 27H_2O$ | 7.0 | 5.5 | 0.7-1.2 | 1.870 | 0.47 | 0.39 | 660 |
| $Na_{86}(AlO_2)_{86}(SiO_2)_{106}]\cdot 264H_2O$ | 6.4 | 4.7 | 1-1.5 | 15.67 | 0.50 | 0.81 | 660 |
| $Na_{56}(AlO_2)_{56}(SiO_2)_{136}]\cdot 250H_2O$ | 5.0 | 3.7 | >1.5-3 | 15.35 | 0.48 | 0.81 | 700 |
| $K_9[(AlO_2)_9(SiO_2)_{27}]\cdot 22H_2O$ | | | 2.6-3.5 | 2.205 | 0.32 | 0.81 | 845 |
| $Na_8(AlO_2)_8(SiO_2)_{40}]\cdot 24H_2O$ | 2.6 | 2.3 | 4.17-5 | 2.794 | 0.28 | 0.39 | |

a. The kinetic diameter represents an intermolecular distance of closest approach for two molecules colliding with zero initial kinetic energy and illustrates the dynamic size of species that can successfully enter through the zeolite pores.
b. Temperature at which structural changes are first noted by X-ray diffraction, for heating in air.

Figure 1.9 shows the two-dimensional representation of the Al-O-Si linkages that create the framework structure of the aluminosilicate zeolites.

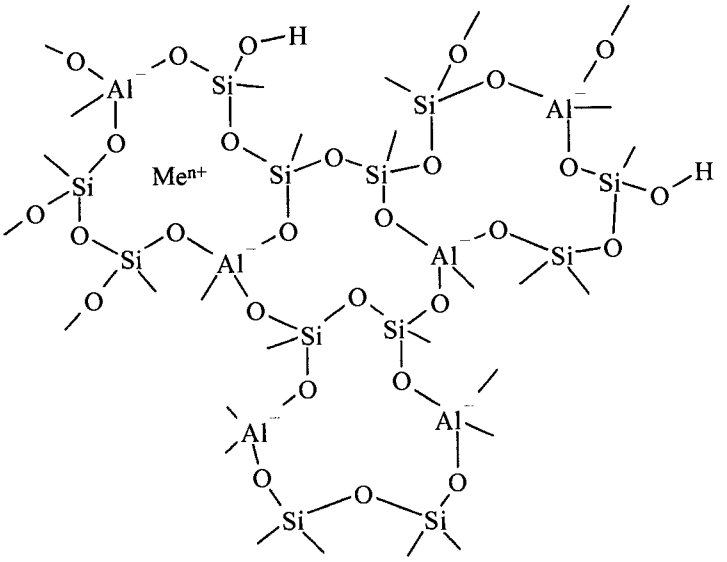


Figure 1.9 Two-dimensional representation of Al-O-Si linkages for the framework structure of aluminosilicate zeolites[46]

The crystals of zeolites are characterized by a three-dimensional pore system, with pores of precisely defined diameter. The corresponding crystallographic structure is formed by tetrahedras of ($AlO_4$) and ($SiO_4$). These tetrahedras are the basic building blocks of various zeolites structures, such as zeolites A, X, Y and mordenite. Due to the presence of alumina, zeolites exhibit a negatively charged framework, which is counter-balanced by positive cations, resulting in a strong electrostatic field on the internal surface. These cations can be exchanged to fine-tune the pore size or adsorption characteristics. For example, the Na-form of zeolite A has a pore opening of

approximately 0.4nm (4Å), it is also known as 4A molecular sieve. If the sodium ion is exchanged with larger potassium ion, the pore opening is reduced to approximately 0.3 nm (3 Å), and the zeolite is called 3A molecular sieve.

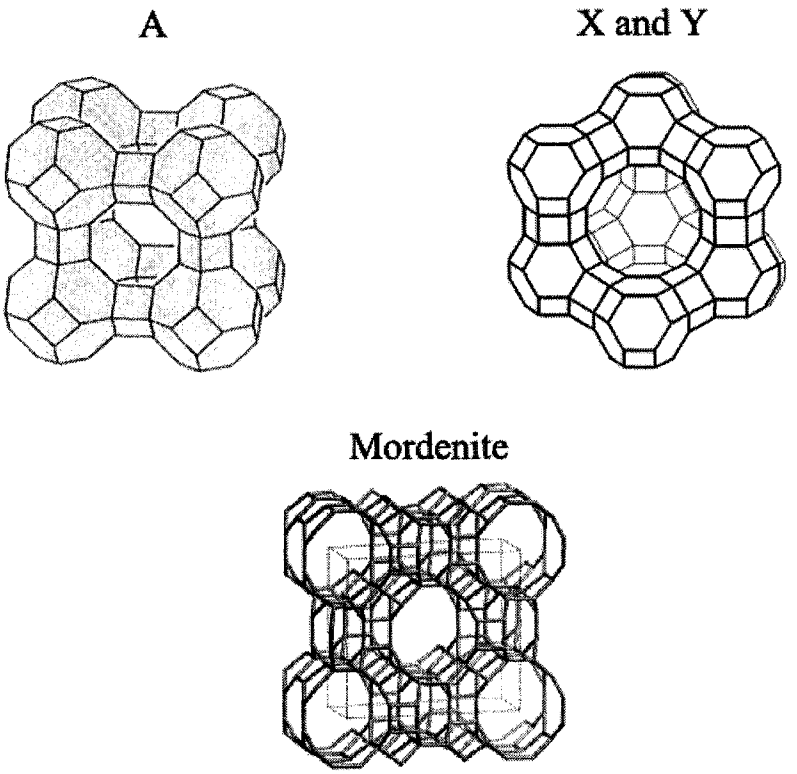


Figure 1.10 Framework structures of zeolites A, X, Y, and mordenite[46]

Zeolite A is a small-pore zeolite (pore diameter 4.1 Å). It can sorb straight chain molecules, such as n-paraffins and olefins and primary alcohols. The cavity of zeolite A is formed by eight truncated octahedral (also call α-cage) and is much larger than the size of the connecting channels (windows). This supercage/window structure is often blamed for the cause of "coke". Large molecules such as aromatics, which are formed in the cage

during the reaction, cannot escape through the narrow window. Therefore, those large molecules are trapped inside the cage and build up coke deposits.

The crystallographic structure of zeolites X and Y is topologically equal to the natural faujasite. Their aluminosilicate skeleton is built, like in case of zeolite A, from cuboctahedron units, but is connected by oxygen bridges formed from six-membered oxygen rings. Each cuboctahedron is joined with 4 additional cuboctahedrons in a tetrahedral arrangement. The elementary cell of zeolites X and Y is formed from 8 cuboctahedrons and 16 oxygen bridges. The adsorption space of big cavities, in the case of faujasite, is surrounded by 10 cuboctahedrons. These cavities are accessible through 4 openings, having a diameter of 7.4 Å and limited by 12-membered oxygen rings, which are characteristic for zeolites X and Y.

Mordenite is a rare zeolite. The crystal structure of mordenite is orthorhombic with straight 12-membered ring channels (6.5 x 7.0 Å) and crossed 8-membered ring channels (2.8 x 5.7 Å). Figure1.10 shows the framework structures of zeolites A, X, Y and mordenite.

Zeolite ZSM-5 is an industrially important catalyst. HZSM-5 is remarkably stable as acidic catalyst. The name is short for Zeolite Socony Mobile and the number 5 for the pore size of 5.6 Å. It exhibits a two dimensional network of channels having a structure as illustrated in Figure 1.11. There are two distinctive pore types intersecting each other. The first of these pores is straight and elliptical in cross section; the second pores intersect the straight pores at right angles, in a zig-zag pattern and are circular in cross section. Because of its unique pore structure, it exhibits a high degree of shape selective catalysis and low coke forming propensity. It has many applications in petroleum refining,

particularly in enhancing the gasoline's octane number, when this zeolite is used as a catalyst additive in gas oil cracking.

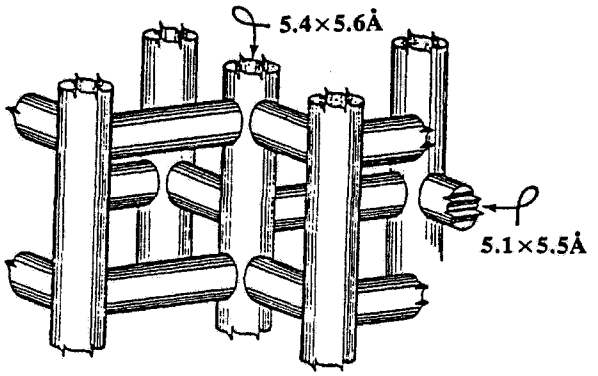


Figure 1.11 Schematic of structure of ZSM-5[23]

The aperture diameters of the above mentioned zeolites are summarized in Table 1.2. As molecular sieves, only adsorbate molecules having a critical diameter smaller than the effective pore diameter of the used zeolite can access its internal adsorption surface.

Table 1.2 Number of oxygen atoms in the ring and aperture diameters of some zeolites

| Zeolite | Number of oxygen in the ring | Aperture diameters, nm |
|---|---|---|
| Zeolite A | 8 | 0.41 |
| Zeolite X,Y | 12 | 0.74 |
| Mordenite | 12 | 0.65x0.70; 0.28x0.57 |
| ZSM-5 | 10 | 0.51x0.55; 0.54x0.55 |

### 1.5.2 Applications of Zeolites and Their Pore Size Limitation

Zeolites have been widely used as catalysts and catalyst supports. There are may reviews on this subject[47,48]. The most successful example of using zeolite as a catalyst is the cracking of gas-oil in fluid catalytic cracking (FCC) unit for the production of gasoline and gas products. Zeolites also play an important role in separation technology as adsorbents or molecular sieves[49,50]. Their adsorption and ion-exchange properties have been applied for the recovery of useful substances and for the removal of pollutants from industrial waste water[51,52]. In most cases of practical applications, only smaller molecules are involved. However, large molecules require mesoporous materials such as MCM-41 and MCF. Unfortunately, these materials are known to be quite thermally and chemically unstable[53,54]. Dealumination of zeolites by AHFS treatments has been proved to be an alternative method for obtaining siliceous mesoporous materials. The obtained products have high thermal and chemical stabilities that are very important for these materials used as catalysts or catalyst supports.

### 1.5.3 Acidity in Zeolites: Brønsted and Lewis Acid Sites

Zeolites in the H-form are solid acid. Their acid strength can be varied over a wide range by modification of the zeolite. There are two types of surface acid sites in zeolites: Brønsted Acid Sites (BAS) and Lewis Acid Sites (LAS).

Brønsted acid sites have bridging hydroxyl groups in SiO(H)Al which are associated with tetrahedrally coordinated or framework Al atoms. These bridging hydroxyl groups can donate protons to adsorbed reactants. Every tetrahedrally coordinated Al atom demonstrates one Brønsted acid site. However, the distribution of Al

in zeolites is non-homogenous. Instead, there is a wide distribution of proton strength in zeolites, which can be detected by Electronmicroprobe Analysis (EPA) and X-Ray photoelectron Spectroscopy[19].

On the other hand, Lewis acid sites contain tricoordinated $Al^{3+}$, which can accept electron pairs from adsorbed reactants. When heated, water is driven off from the zeolite structure and Brønsted acid sites will convert into Lewis acid sites. Inversely, Lewis acid sites can be saturated by water and re-converted to Brønsted acid sites. Figure 1.12 shows the conversion of Brønsted acid and Lewis acid sites.

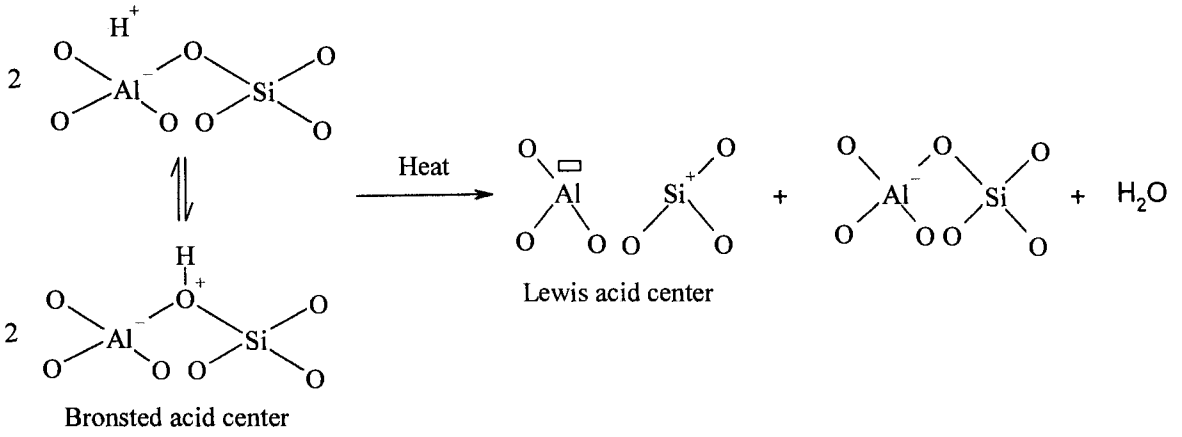


Figure 1.12 Conversion of Brønsted acid site and Lewis acid site[55]

### 1.5.4 $SiO_2/Al_2O_3$ Ratio in Zeolites

In general, the $SiO_2/Al_2O_3$ ratio of a zeolite is determined by the composition of the synthesis mixture and synthesis conditions. However, this ratio can be modified by chemical dealumination[56-61] or desilication[62,63]. The framework $SiO_2/Al_2O_3$ ratio is directly related to the number of $AlO_2^-$ sites, in other word, the number of acid sites. Therefore, the $SiO_2/Al_2O_3$ ratio has a major influence on the acidity of the zeolite. Table 1.3 shows the Si/Al ratio and the associated acid/base properties. The $SiO_2/Al_2O_3$ ratio is also used to denote the hydrophobicity of zeolites, with higher ratio indicating a higher degree of hydrophobicity and lower ion-exchange capacity.

Table 1.3 Classification of acidic zeolite to increasing Si/Al ratio[55]

| Si/Al ratio | Zeolite | Acid/base properties |
|---|---|---|
| Low (1-1.5) | A, X | relatively low stability of lattice;<br>low stability in acids;<br>high stability in bases;<br>high concentration of acid groups of medium strength |
| Medium (2-5) | erionite<br>chabazite<br>Mordenite<br>Y | |
| High(ca. 10 to ∞) | ZSM-5<br>dealuminated<br>erionite, mordenite, Y | relatively high stability of lattice;<br>high stability in acids;<br>low stability in bases;<br>low concentration of acid groups of medium strength |

### 1.5.5 Dealumination of Zeolites

Modification of zeolites, such as by dealumination, desilication, or by using methods called pore size engineering[64], will partially change the structural, compositional, acidic and/or ion-exchange characteristics. These techniques have been used in improving the properties of zeolites post-synthetically for some special purposes.

The methods of dealumination include chemical treatments and hydrothermal treatment. In chemical treatments, the more frequently used methods are acid treatment and treatment with ammonium hexafluorosilicate (AHFS). In the early stage, these techniques were essentially applied to zeolites with high Si/Al ratio with the intention to modify the Al content of the zeolite surface without provoking either total or partial structure collapse.

In 1992, Le Van Mao et al. found that by using dealumination techniques under carefully controlled and relatively mild conditions for treating alumina-rich zeolite, such as Ca-A zeolite, it is possible to produced mesoporous materials with rather narrow size distribution, showing a maximum at 12-14nm[57]. The main technique essentially involves the AHFS treatment, which is also known as secondary synthesis. The involved reaction was as follows:

$$AlO_4^- + (NH_4)_2SiF_6 = SiO_4 + (NH_4)_2AlF_5 + F^- \qquad (1\text{-}1)$$

The average pore size depends on the rate of addition of the AHFS solution to the leaching medium. If such a treatment is combined with acid leaching or hydrothermal treatment, the mesoporous materials obtained exhibit similar pore size distribution but their adsorption capacity for nitrogen is significantly increased. This may be an alternative line of research for preparation of siliceous mesoporous materials.

Further investigations by Le Van Mao et al showed that for zeolite X, leaching by AHFS under controlled conditions also resulted in pore size enlargement, forming mesoporous aluminosilicates (with average pore size varying from 3 to 5 nm)[58]. According to comparative studies using hydrothermal treatment, HCl leaching treatment and AHFS leaching treatment for Ca-A zeolite pore size enlargement[59], they found that the mild acid leaching and the hydrothermal treatment led to mesoporous materials with a sharp distribution of pore size in the 4 nm region. It is worth noting that mesopores of ca. 4 nm in size already exist in the parent Ca-A zeolite, but in a very low amount. However, treatment by AHFS leaching resulted in materials with mesopores of ca. 12 nm in size. Such mesopores do not exist in the parent Ca-A zeolite. Moreover, the curves of mesopore size distribution are not as sharp as in the cases for acid and hydrothermal treatments. By changing the temperature for AHFS treatment from room temperature to 80°C, a significantly flattened curve of the pore size distribution will be observed.

Compared with their parent zeolites, the mesoporous materials obtained by pore enlargement have slightly lower surface area and unique pore structure, with pore size of nanoscale range. These materials may have potential advantages in practical application for their special pore features.

Though mechanism of mesopore formation by dealumination of zeolites is not so clear for now, some suggestions have been made by Le Van Mao et al. based on their observations[59].

It has been proved that for alumina-rich zeolites, such as zeolites A and X, dealumination resulted in pore size enlargement[65], but for zeolites with higher Si/Al ratio, such as Y zeolite, no significant pore size enlargement was observed by similar

treatments. These facts indicate that pore size enlargement is a result of the removal of alumino-silicate "clusters" from the zeolites framework by extraction of Al atoms which actually defined the cleavage line of the clusters. Since an alumina-rich zeolites can supply more Al-cleavage points, the removal of such clusters appears favored to such a zeolite.

Acid leaching and hydrothermal treaments of A and X zeolites and AHFS treatment of X zeolite result in solids having 3.5 nm-size mesopores, which already exist in the parent zeolites, although in very low amounts. It is believed that "cluster" removal is initiated at a certain level of coverage of the parent zeolites wall by the corrosive reagents. Such an effective level of coverage can be attained only in the original mesopores, which are capable of adsorbing a large number of reactant molecules. Pore enlargement of zeolite A by AHFS that result in larger mesopores probably is initiated in a similar way.

Pore enlargement by AHFS seems to be less destructive than other techniques mentioned above. As can be seen from equation (1-1), the possibility of having some of the extracted Al atoms replaced by Si atoms of the AHFS molecules, reinforces the remaining structure.

For size selectivity and size exclusion effects, both pore size and pore shape may play key roles. To investigate nitrogen adsorption/desorption isotherm will provide an insight into the pore shape features[66,67]. It is customary to express the average width of the pores of a porous substance as:

$$r_m = 2 V_p / S \qquad (1\text{-}2)$$

where $r_m$ is the mean value of the radius of the pores, $V_p$ is the pore volume, and S is the total surface area. This conventional expression is based on the assumption that all pores are cylindrically shaped, having a radius of cross section $r_m$ and a pore length L. An idealization of the pore system to cylindrically shaped capillaries, which are open on both sides, offers an explanation for the occurrence of hysteresis phenomena in capillary condensation. The pores are filled (on the adsorption branch) when the relative vapour pressure ($p_a/p_o$) of the adsorbate reaches the value:

$$(p_a/p_o) = \exp ( - 2\sigma V_m \cos\alpha / RT \cdot 2r) \qquad (1\text{-}3)$$

where $\sigma$ is the surface tension and $V_m$ is the molar volume of the adsorbate, r is the radius of the pore and $\alpha$ is the angle of wetting. They are emptied (on the desorption branch) when

$$(p_a/p_o) = \exp ( -2\sigma V_m \cos\alpha / RT \cdot r) \qquad (1\text{-}4)$$

The adsorbate desorption, after saturation is reached, is the opposite of the adsorption, but evaporation from pores usually takes place at a pressure lower than that of capillary condensation, giving a hysteresis. This is due to pore shape, and four types of hysteresis in nitrogen adsorption/desorption isotherm have been recognized (See Figure 1.13).

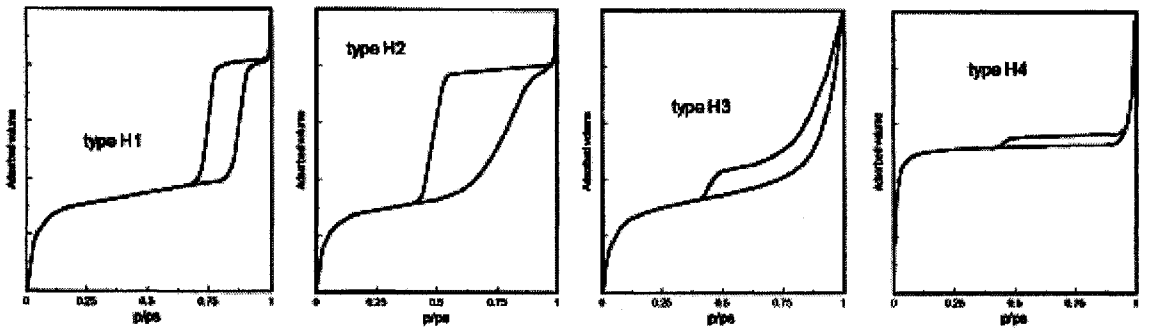


Figure 1.13 Four hysteresis shapes of adsorption isotherm usually found by nitrogen adsorption[67]

Types H1 and H2 hysteresis are characteristic of solids consisting of particles crossed by nearly cylindrical channels or made by aggregates (consolidated) or agglomerates (unconsolidated) of spheroidal particles. In both cases, the pores can have uniform size or shape (type H1) or non-uniform size or shape (type H2). Hysteresis shown in H1 is usually attributed to different size of pore mouth and pore body (this is the case of ink-bottle pores) or to a different behaviour in adsorption and desorption in near cylindrical through pores.

Types H3 and H4 hysteresis are usually found on solids consisting of aggregates or agglomerates of particles forming slit shaped pores with uniform (type H4) or non-uniform (type H3) size and/or shape.

No hysteresis is corresponding to the case of blind cylindrical, cone-shaped and wedge-shaped pores, or to some cases discussed in ref [66].

In ref [66] more special cases of the hysteresis were included, and correspondingly many shape groups were discussed. Thus, based on the type of the

hysteresis loop we can estimate the pore shape of the resulting product obtained from pore enlargement.

From the type of adsorption isotherm, we can also obtain some information about the pore size of the porous materials. Figure 1.14 shows the four types of the adsorption isotherms that are usually found in catalyst characterization:

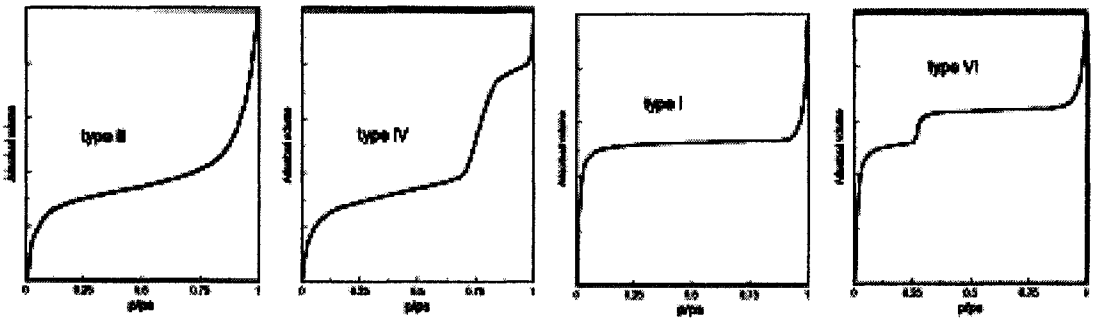


Figure 1.14 Four types of adsorption isotherm usually found by nitrogen adsorption[67]

Macroporous solids (type II);

Mesoporous solids (type IV);

Microporous solids (type I);

Uniform ultramicroporous solids (type VI).

## 1.6 The Objectives of This Research

In recent years, catalyst R&D is more focused on the production of light olefins, namely ethylene and propylene, and secondarily of BTX aromatics. Therefore, this research aims at finding the suitable catalysts and the best reaction conditions in order to selectively produce hydrocarbons especially ethylene and/or propylene from aqueous ethanol obtained by fermentation.

The conversion of ethanol into hydrocarbons can only be carried out by acidic catalysts. In the past, several acidic catalysts were tested by Dr. Le Van Mao's group and zeolite catalysts appeared to be very efficient catalyst for the conversion of ethanol into hydrocarbons due to their strong acidity. Their results also indicated that the yield of light hydrocarbon increases significantly when incorporating trifloromethanesulfonic acid (triflic acid or TFA) into zeolite ZSM-5 (in acid form). Since the pore size of ZSM-5 is very small only 5.6 Å, the amount of TFA incorporated is quite limited, and thus many researchers pay more attention to mesoporous material. Two types of silica nanoboxes were developed by Dr. Le Van Mao's group: silica nanoboxes by dealumination of A or X zeolites and silica nanoboxes by desilication of ZSM-5 zeolite. It has been found that silica nanoboxes have high thermal and chemical stabilities. Obviously, these physical and chemical properties of silica nanoboxes may be advantageous in use as catalysts or catalyst supports or matrices.

The first objective of this thesis is to study the first type silica nanoboxes, investigate the influence of experimental conditions on the textural properties of the porous products in dealumination by AHFS treatment and then incorporate TFA with this type of silica nanoboxes.

The second part of this thesis is to submit silica nanoboxes, silica nanoboxes incoporated with TFA, and those known acidic zeolite catalysts such as HY, H-UYS(ultra stable Y zeolite in acidic form) and HZSM-5 into the production of hydrocarbons from aqueous ethanol process. Silica nanoboxes prepared in our laboratory are expected to be a very promising solid acidic catalyst.

# Chapter 2 Experimental

## 2.1 Materials and Reagents

The chemicals and zeolite materials used in catalytic testing and characterization in this research work were purchased from several suppliers as the following:

| Chemicals | Suppliers |
|---|---|
| NaA Zeolite (Type 4A), powder | Linde Union Carbide |
| NaX Zeolite (Type 13X), powder | Linde Union Carbide |
| $NH_4Y$ Zeolite (Type LZY-82), powder | UOP Company |
| Na form Modenite Zeolite, powder | Zeochem AG |
| H-DeX, powder | Prepared in our laboratory |
| H-Y Zeolite, powder | UOP Company |
| H-USY Zeolite (Ultra Stable Y Type), powder | UOP Company |
| H-ZSM-5, powder | Zeochem AG |
| Bentonite, Technical grade | Aldrich Chemical Company, Inc. |
| Silica-alumina, powder | Aldrich Chemical Company, Inc. |
| Ammonium acetate, ≥98.0% | Fisher Scientific Inc. |
| Ammonium chloride, Technical grade | ACP Chemicals Inc. |
| Ammonium fluoride, 98+% | Aldrich Chemical Company, Inc. |
| Ammonium hexafluorosilicate (AHFS), 99% | Stream Chemicals |
| Aluminum reference solution (1000ppm+/-1%) | Fisher Scientific Inc. |

| | |
|---|---|
| 2-Butanol, 99+% | Aldrich Chemical Company, Inc. |
| di-Ethyl ether, 99+% | Aldrich Chemical Company, Inc. |
| Ethanol, 99% | Aldrich Chemical Company, Inc. |
| n-Hexane, 99+% | Aldrich Chemical Company, Inc. |
| Hydrochloric acid | Fisher Scientific Inc. |
| Hydrogen peroxide solution, 30 wt% | Aldrich Chemical Company, Inc. |
| Lithium tetraborate | Aldrich Chemical Company, Inc. |
| Potassium carbonate | Aldrich Chemical Company, Inc. |
| Sodium hydroxide | Fisher Scientific Inc. |
| Triflormethanesulsonic acid, 99+% | Stream Chemicals |

## 2.2 Dealumination of Zeolites by AHFS Treatment

Procedure 1:

According to procedure 1, the dealumination of zeolites by AHFS treatment was carried out in the manner similar to that reported in refs. [57-59]. Typically 2.7g of NaX zeolite (powder form) were placed into a Teflon beaker containing 200 $cm^3$ of 0.8 $mol \cdot dm^{-3}$ ammonium acetate solution (pH 7.0). Then 20 $cm^3$ of freshly prepared AHFS solution(0.5 $mol \cdot dm^{-3}$) were added to the suspension using an injection syringe on an infusion pump, under mild stirring by a magnetic stirrer. The rate of AHFS addition was kept at 0.81 $cm^3 \cdot min^{-1}$. Slow stirring was continued for 1 hour at 80°C in the water bath after the AHFS addition was completed. The solid was then separated by filtration and washed on the filter for five times, each with ca. 300 $cm^3$ of distilled water. The product was dried in an oven at 110°C overnight in the air and then the agglomerates were ground in a mortar. The fine powder was stored for use.

In investigations of the experimental condition effects, the amount of parent zeolites added, the amount of AHFS used, the rate of AHFS addition, the temperature of the water bath and the stirring time in the water bath were partially varied in the experiments.

Procedure 2:

Into a certain amount (5.0g or 10.0g) of NaX zeolite, 0.05 $mol \cdot dm^{-3}$ AHFS solution (containing 0.8 $mol \cdot dm^{-3}$ ammonium acetate, pH 7.0) was added under stirring at room temperature. The amount of AHFS added was $3.0 \times 10^{-3}$ mol/g zeolite. Then the mixture contained in a beaker was placed into a water bath at 50°C for 1 hour with mild

stirring. The solid was then separated by filtration and washed on the filter for five times, each time with ca. 300 $cm^3$ of distilled water (or more, depending on the amount of zeolite used). The zeolite slurry was boiling in 2L of water for 1 hour with vigorous stirring, then filtered and washed with hot water, and the product was dried in an oven at 110°C overnight in the air. Finally the agglomerates were ground in a mortar and the fine powder was stored for use.

## 2.3 Characterization of Silica Nanobox

### 2.3.1 Acidity Investigation

The acidity (strength and density) of the zeolites was studied by $NH_3$-TPD-ISE method, which was developed by Dr. Le Van Mao's group[68]. The sample was carried out in a fixed-bed reactor equipped with a programmable temperature controller at ambient pressure. 1.0 g of sample was loaded into the reactor then they were preheated at 300°C for 3 hours in flowing dehydrated nitrogen at a flow rate of 60.0 $cm^3 \cdot min^{-1}$. After cooling to 100°C, they were exposed to stream of dehydrated ammonia for 1 hour at a flow rate of 20.0 $cm^3 \cdot min^{-1}$. Then, the sample was left in flowing nitrogen at the same temperature for 6 hours in order to purge any excess and/or weakly adsorbed ammonia. Finally, the TPD measurement was performed from the purging temperature to 650°C at a heating rate of 15.0°C $\cdot min^{-1}$. The desorbed ammonia was detected with an ammonium ion-selective electrode ($NH_4^+$-ISE) attached to a pH 2100 meter with a digital display.

### 2.3.2 BET (Brunauer Emmet and Teller)

Characterization techniques included the determination of the textural properties, such as the nitrogen adsorption/desorption isotherm, the BET surface area, the pore size distribution (using BJH nitrogen adsorption/desorption method) and the average pore diameter. The equipment used was a Micromeretic ASAP Model. It should be pointed out that in the present work the IUPAC nomenclature for the pores based on their diameters is adapted, that is, micropores or "zeolite-type micropores" (<2nm), mesopores (2-50nm) and macropores (>50nm). Unfortunately, with Micromeretic ASAP Model system mespores and macropores with pore size from 1.7 to 300nm can be characterized, and the mesopore size distribution can only be determined based on the volume of nitrogen adsorbed and then desorbed per gram of solid material. In addition, the amounts of micropores were estimated using the volume of nitrogen adsorbed and then desorbed by the pore which has size smaller then 1.7nm ($V_{mic}$). It was assumed that the micropores of the aluminosilicates obtained were of the zeolite type. The pore size distribution was investigated by plotting the differential pore volume (F = dV/dlog10 D) as a function of the pore diameter D, where V is pore volume; V and D are in $cm^3$ and nm, respectively.

### 2.3.3 DTA/TGA Thermal Analysis

TGA is a technique in which the mass of a substance is measured as the temperature of the substance is varied. Changes in the mass reflect a decomposition or oxidation in the air of the substance. DTA detects the temperature changes between the sample and an inert reference material during a programmed change of temperature, involving an exchange of energy ($\Delta H \neq 0$), e.g. chemical change or first order phase

transition. The peaks on the DTA curve show us either exothermic or endothermic process takes place in the sample upon heating, combined with the TGA curve, we can determine whether a chemical reaction or a first order phase transition (including classical types and solid state phase transition) occurs[69].

In this research work, DTA/TGD thermal analysis technique was used to determine the thermal stability of acid form dealuminated zeolite X and also the amount of TFA incorporated on this zeolite.

### 2.3.4 Determination of $SiO_2/Al_2O_3$ Ratio

In order to determine the aluminum concentration and $SiO_2/Al_2O_3$ ratio of the dealuminated zeolite, a weighed amount of solid sample was first dissolved in acid solution. The fusion melting method was developed in Dr. Le Van Mao's group[69] for sample preparation.

The analysis of the chemical compositions in samples ($Al_2O_3$, $SiO_2$) was carried out on a Perkin-Elmer model 2380 Atomic Absorption Instrument. Aluminum hollow cathode lamp and nitrous oxide burner were used for the analyses.

### 2.3.5 Hydrothermal Stability Testing

Hydrothermal stability test was carried out as follows: Silica nanoboxes product, such as DeX or $DeNH_4X$, were calcined at 300°C for 3 hours and then at 600°C for 3 hours (expressed as DeNaX-c or H-DeX-c). To the calcined silica nanoboxes sample, weighed amount of Bentonite (nanoboxes sample: 80 wt% and Bentonite: 20 wt%) and a

small amount of water was added, mixed well and extruded into rod-shaped material and left in an oven (110°C) overnight, then cut into small pieces (Φ1.5mmx2-3mm). This product (expressed as DeNaX-m or H-DeX-m) was treated at 600°C for 3 hours, and was used as the final sample for hydrothermal stability test. 2 g of the final sample was placed into a quartz tubular reactor (40cmx1cm I.D.). Catalyst bed temperature was kept at 500°C. Nitrogen gas and steam were introduced into the reactor (nitrogen flow rate: 5 $cm^3 \cdot min^{-1}$, and $H_2O$ injected rate: ca. 0.565 $cm^3 \cdot min^{-1}$). The weight hourly space velocity (WHSV) was 1.7 $h^{-1}$. The time for this treatment was 5 hours and the total volume of $H_2O$ injected was 16.2 $cm^3$. The hydrothermal treated sample is expressed as DeNaX-h or H-DeX-h. Before and after hydrothermal treatment, textural properties of the sample were determined by BET investigation.

## 2.4 Preparation of Catalysts

### 2.4.1 Preparation of Acid Form Zeolites

The ammonium form zeolite was prepared by repeated ion-exchange of the sodium form with a 5 wt% solution of ammonium chloride at 80°C under mild stirring (1.0g of solid for 10 $cm^3$ of solution). Each treatment lasted 2 hours, after which the used solution was decanted and fresh solution was added. This procedure was repeated two more times. The resulting solid was then filtered out, washed with water and dried overnight in the air at 110°C. The acid form zeolite was generated by activating the sample in the air at 300°C for 3 hours, and then at 600°C for 3 hours.

### 2.4.2 Loading the Triflic Acid into H-DeX

Triflic acid (Trifloromethanesulfonic acid) is one of the strongest acids known. As described in ref. [70], well-defined quantity of aqueous solution of triflic acid (0.0149 $g \cdot cm^{-3}$) was added to 10 g of H-DeX sample to achieve 15 wt% of acid loading. The suspension was then placed in the fume hood at room temperature to evaporate all the water for more than 5 hours. The apparently dried solid was further dried in the oven at 110°C in the air overnight. The prepared product is denoted as H-DeX-15%TFA.

### 2.4.3 Preparation of Catalyst Extrudates

To H-DeX-15%TFA sample, given amount of Bentonite (nanoboxes sample: 80 wt% and Bentonite: 20 wt%) and a small amount of water were added, mixed well and extruded into rod-shaped material and left in an oven (110°C) overnight, then cut into small pieces (Φ1.5mmx2-3mm). This catalyst was active at 250°C for 3 hours (expressed as 15%-TFA). For comparison, H-DeX, H-ZSM-5, H-USY and H-Y zeolites were also adopted in catalytic dehydration of ethanol. They were all mixed with Bentonite(20 wt%), respectively, and were treated in the same manner as for the preparation of 15%-TFA except those catalysts were active at 400°C for 3 hours.

## 2.5 Catalytic Testing

Using the prepared catalysts in the dehydration of ethanol, the catalytic runs were performed as follows[3]:

Ethanol or its aqueous solutions was introduced into an alcohol vaporizer-gas mixer by using an injection syringe on an infusion pump. Nitrogen gas was supplied to

the mixer from a cylinder, connected in-line with a flow-meter. The nitrogen gas then carried the vaporized alcohol feed through a catalyst bed set in a catalytic reactor contained inside a furnace, which was thermo-regulated. The reaction temperature was monitored by a thermocouple (placed in the catalyst bed), in conjunction with a digital thermometer unit. The gaseous mixture flowing out of the reactor ran through a series of condensers and then ran into a liquid collector immersed in an ice bath. A dynamic gas sampling bulb, from which gas sampling was carried out, direct connected on the liquid collector. The gas effluent was analyzed by gas chromatography (GS-alumina capillary column, 50m, with flame ionization detection) using a normalization method for quantization, then selectivity for ethylene and other hydrocarbons was calculated. The collected liquid was weighed and determined by gas chromatography (Chrom254 packed column, 2m, with flame ionization detection) using 2-butanol as internal standard. In this way conversion of ethanol was obtained.

The reaction conditions used in the experiments were as follows: Reaction temperatures were ranged from 150 to 350°C for different experiments; catalyst weight was 2g; flow rate of nitrogen was 10 $cm^3 \cdot min^{-1}$; weight hourly space velocity (WHSV) was 1 to 5 $h^{-1}$; duration of a run was 4 hours. GC analysis was conducted every hour, and the mean of the four results was reported.

# Chapter 3 Results and Discussion

## 3.1 Experimental Conditions Effect in Preparatoin of Silica Nanoboxs by AHFS Dealumination

### 3.1.1 Dealumination of Zeolite NaX

It has been reported that mesoporous material can be prepared by AHFS treatment of zeolite X[68]. For example, 2.7g of NaX zeolite react with AHFS in a buffer solution at room temperature for 3 hours; the resulting mesopores are concentrated within the 3 - 5 nm range. In this work, based on procedure 1, 4.0 to 5.0 g of NaX zeolite was used as starting material, and experimental condition effects on the textural properties of the resulting products were investigated in detail. Table 3.1 indicates the influence of reaction temperature on textural properties of the product. It is obvious that with increasing reaction temperature from room temperature to 80°C, average pore diameter increases from 3.1 nm to 4.9 nm, and BET surface area decreases from 333.1 to 302.5 $m^2 \cdot g^{-1}$. At the same time the volume of $N_2$ adsorbed slightly increases. The plot of pore size distribution for the sample obtained at 80°C shows two peaks; however, narrow pore size distribution (single peak) can be observed at lower reaction temperatures. Figure 3.1 is the plot of pore size distribution for the sample obtained at 70°C.

Table 3.1 Influence of reaction temperature on the textural properties of dealumination of NaX zeolite

| Sample ID | $S_{BET}$ $m^2/g$ | $D_{av.}$ nm | $V_t$ cc/g | $V_{mic}$ cc/g | Desorption pore volume plot |
|---|---|---|---|---|---|
| DeNaX-T1 RoomTem | 326.4 | 3.1 | 0.25 | 0.01 | 1peak |
| DeNaX-T2 60°C | 333.1 | 3.7 | 0.31 | 0 | 1peak |
| DeNaX-T3 70°C | 363.1 | 3.8 | 0.35 | 0 | 1peak |
| DeNaX-T4 80°C | 302.5 | 4.9 | 0.37 | 0 | 2peaks |

Note: 4.0 g of zeolite were used. Injection rate: 1.1 $cm^3 \cdot min^{-1}$; amount of AHFS added: 20ml; reaction time: 1hour.

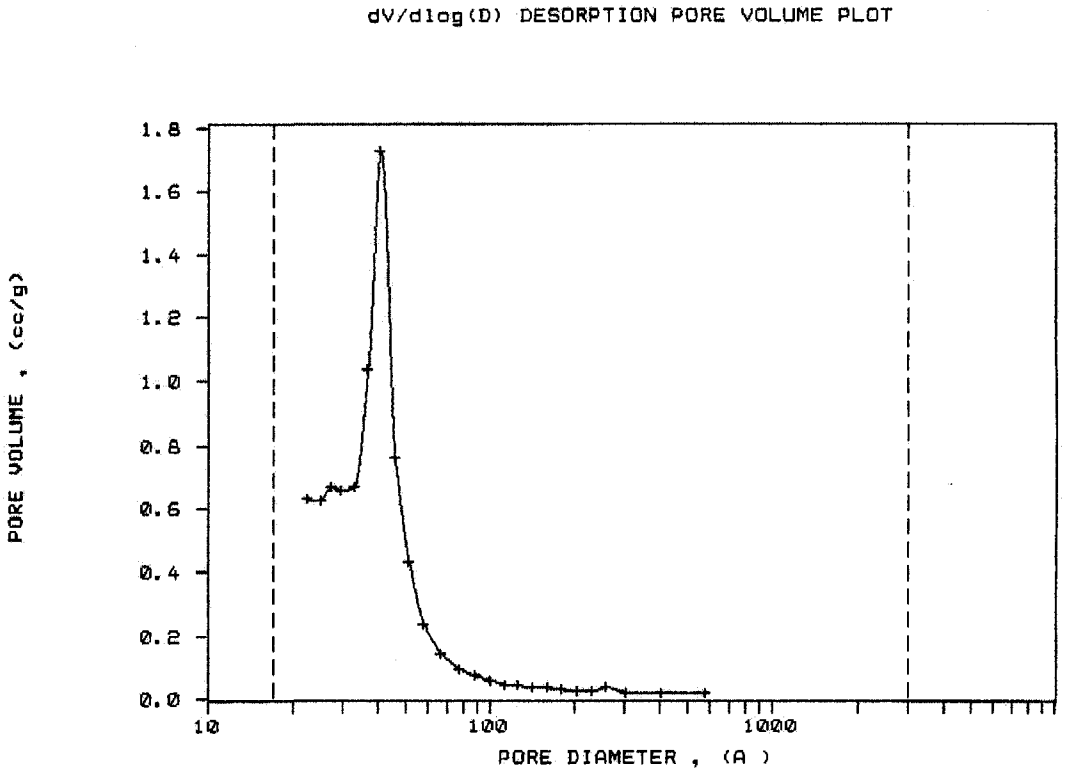


Figure 3.1 Pore size distribution for DeNaX sample obtained at 70°C

Table 3.2 gives the experimental results obtained in different AHFS addition rates. It seems that as changing the AHFS addition rate from 0.8 to 1.5 $cm^3 \cdot min^{-1}$, there is no significant effect on the textural properties. Therefore, the AHFS addition rate is not a key factor for changing the textural properties of dealuminated X zeolite.

Table 3.2 Influence of AHFS addition rate on the textural properties of the dealumination of NaX zeolite

| Sample ID | $S_{BET}$ $m^2/g$ | $D_{av.}$ nm | $V_t$ cc/g | $V_{mic}$ cc/g | Desorption pore volume plot |
|---|---|---|---|---|---|
| DeNaX-R1 Rate:0.8ml/min | 298.3 | 5.0 | 0.37 | 0 | 2peaks |
| DeNaX-R2 Rate:1.2 ml/min | 317.1 | 4.9 | 0.39 | 0 | 2 peaks |
| DeNaX-R3 Rate:1.5ml/min | 306.2 | 5.0 | 0.38 | 0 | 2 peaks |

Note: 4.0 g of zeolite X were used. Amount of AHFS added was 20ml; reaction temperaturewas 80 °C; reaction time was 1 h.

Table 3.3 shows the influence of reaction time on textural properties of the product. It can be seen that with increasing reaction time from 1 h to 5 h, average pore diameter increases from 3.0 nm to 3.6 nm, and BET surface area decreases from 482.4 to 354.7 $m^2 \cdot g^{-1}$. At the same time the volume of $N_2$ adsorbed decreases.

Table 3.3 Influence of reaction time on the textural properties of the dealumination of NaX zeolite

| Sample ID | $S_{BET}$ $m^2/g$ | $D_{av.}$ nm | $V_t$ cc/g | $V_{mic}$ cc/g | Desorption pore volume plot |
|---|---|---|---|---|---|
| DeNaX-H1 1hour | 482.4 | 3.0 | 0.37 | 0.08 | 1peak |
| DeNaX-H2 2 hours | 434.1 | 2.9 | 0.31 | 0.08 | 1peak |
| DeNaX-H3 3 hours | 391.0 | 3.3 | 0.31 | 0.05 | 1peak |
| DeNaX-H4 4 hours | 427.5 | 3.2 | 0.35 | 0.06 | 1peak |
| DeNaX-H5 5 hours | 354.7 | 3.6 | 0.32 | 0.03 | 1peak |

Note: 5.0 g of zeolite X were used. Amount of AHFD added was 20 ml; injection rate was 1.3 $ml \cdot min^{-1}$; reaction temperature was room temperature.

Results in Table 3.4 show that with increasing the amount of AHFS added, the total pore volume and the average pore diameter of the product regularly increase. Compared sample DeNaX-A1 in Table3.4 with sample DeNaX-H5 in Table 3.3, we can find that prolonging the reaction time also results in increasing the total pore volume and average pore size. Moreover, it can be seen from Table 3.3 and 3.4 that by AHFS treatment at room temperature, in most cases the original zeolite micropores cannot be completely eliminated.

Table 3.4 Influence of AHFS addition amounts on the textural properties of the dealumination of NaX zeolite

| Sample ID | $S_{BET}$ $m^2/g$ | $D_{av.}$ nm | $V_t$ cc/g | $V_{mic}$ cc/g | Desorption pore volume plot |
|---|---|---|---|---|---|
| DeNaX6-A1 AHFS:20ml | 409.2 | 3.1 | 0.32 | 0.05 | 1peak |
| DeNaX6-A2 AHFS:25ml | 349.1 | 4.0 | 0.35 | 0.03 | 2peaks |
| DeNaX6-A3 AHFS:30ml | 324.7 | 4.3 | 0.35 | 0.02 | 2peaks |

Note: 6.0 g of zeolite X were used. Injection rate was 1.3 ml $min^{-1}$; reaction temperature was room temperature; reaction time was: 3 h.

With a better understanding the key factors that affect the textural properties of the product, we can prepare the mesoporous materials from zeolite X by controlling experimental conditions. Reproducibility tests were conducted (See Table 3.5). It can be seen that under strictly controlled operation conditions only a minor fluctuation in textural properties is observed. The relative standard deviations for surface area, pore size and total pore volume for 5 samples prepared under the same conditions are 1.5%, 3.2% and 2.4%, respectively.

Table 3.5 Reproducibility test for dealumination of NaX zeolite

| Sample ID | $S_{BET}$ $m^2/g$ | $D_{av.}$ nm | $V_t$ cc/g | $V_{mic}$ cc/g | Desorption pore volume plot |
|---|---|---|---|---|---|
| 1 | 363.1 | 3.8 | 0.35 | 0 | 1peak |
| 2 | 366.9 | 3.8 | 0.34 | 0 | 1peak |
| 3 | 375.0 | 3.6 | 0.34 | 0 | 1peak |
| 4 | 362.6 | 3.9 | 0.36 | 0 | 1peak |
| 5 | 361.1 | 3.9 | 0.35 | 0 | 1peak |

Note: 4.0 g of zeolite X were used. Injection rate was 1.1 ml·$min^{-1}$; reaction temperature was 70°C; reaction time was 1 h.

In order to obtain significant amount of mesoporous materials for the further catalytic activity testing, the scale of the pore enlargement process must be extent. Therefore, more investigations on experimental conditions should be carried out. As far as our experience, to scale up the pore enlargement process and to obtain a product of desired quality cannot be effected by simply increasing the reactants proportionally based on procedure 1. In order to facilitate scaling up the selected preparation process, here we adopt procedure 2, as described in Experimental section. Experimental results (See Table 3.6) based on procedure 2 showed that, for preparation of silica nanoboxes from NaX zeolite by AHFS treatment, the optimal conditions are: Concentration of AHFS = 0.05 $mol \cdot dm^{-3}$; the amount of AHFS added = 2.5~3.0 x $10^{-3}$ $mol/g^{-1}$ zeolite; reaction temperature = 50~60°C; reaction time = 1 h.

Table 3.6 Textural properties for dealumination of NaX zeolite

| Sample ID | $S_{BET}$ $m^2/g$ | $D_{av.}$ nm | $V_t$ cc/g | $V_{mic}$ cc/g | Desorption pore volume plot |
|---|---|---|---|---|---|
| 5G | 357.1 | 4.2 | 0.37 | 0 | 1peak |
| 10G | 351.2 | 4.6 | 0.41 | 0 | 1peak |

Note: 5G indicates 5.0 g of zeolite X used as starting material; 10G indicates 10.0 g zeolite X used as starting material.

It is worth to point out that boiling the crude product in water to remove the adsorbed impurities is essential for assuring high thermal stability of the final product. As shown in Table 3.7, Sample-1 was prepared according to the procedure 2 described in the Experimental section, and Sample-3 was prepared by the same procedure except the "boiling in water" step; Sample-2 and Sample-4 were obtained from Sample-1 and Sample-3 by calcining at 300°C for 3 hours and then at 600°C for 3 hours respectively. It

can be seen that after calcining, the pore structure of Sample-3 severely collapsed, and the textural properties of Sample-1 only changed slightly.

Table 3.7 Textural properties for dealumination of NaX zeolite

| Sample ID | $S_{BET}$ $m^2/g$ | $D_{av.}$ nm | $V_t$ cc/g | $V_{mic}$ cc/g | Desorption pore volume plot |
|---|---|---|---|---|---|
| Sample-1 | 357.1 | 4.2 | 0.37 | 0 | 1peak |
| Sample-2 | 253.7 | 4.8 | 0.3 | 0 | 1peak |
| Sample-3 | 382.6 | 3.7 | 0.36 | 0 | 1peak |
| Sample-4 | 57.5 | 8.4 | 0.12 | 0 | 1broad peak |

### 3.1.2 Dealumination of Zeolite NaA

It has been proved that for alumina-rich zeolites, such as CaA and NaA zeolites, pore enlargement can be easily effected by AHFS treatment based on procedure 1[57-59]. As NaA zeolite is selected as starting material, under conditions similar to previous work but with larger amount of zeolite treated (increasing from 3g to 4g), results obtained are shown in Table 3.8.

It can be seen from these results that after AHFS treatment under different conditions the micropores nearly disappear in the resulting products. Increasing reaction temperature from room temperature to 70°C results in an increase of average pore diameter from 11.0 nm to 15.8 nm, and a decrease of the BET surface from 242 to 189 $m^2 \cdot g^{-1}$.

The pore size distribution for sample DeNaA-2 is presented in Figure 3.2. In each case for the four samples, only a single peak reveals. Hysteresis loops in nitrogen

adsorption/desorption isotherm were also investigated. With changing the experimental conditions in our case no significant change in hysteresis loop was observed. That is, as NaA zeolite is used as starting material, though experimental conditions change in some extent, pore shapes actually remain unchanged.

Table 3.8 Textural properties for dealumination of NaA zeolite

| Sample ID | $S_{BET}$ $m^2/g$ | $D_{av.}$ nm | $V_t$ cc/g | $V_{mic}$ cc/g | Desorption pore volume plot |
|---|---|---|---|---|---|
| DeNaA-1 AHFS:18ml Rate:1.1 ml/min RoomTem-1hr | 237.0 | 10.5 | 0.62 | 0 | 1peak |
| DeNaA-2 AHFS:20ml Rate:1.1 ml/min RoomTem-1hr | 242.1 | 11.0 | 0.66 | 0 | 1peak |
| DeNaA-3 AHFS:20ml Rate:1.1 ml/min 70°C-1hr | 189.4 | 15.8 | 0.75 | 0 | 1peak |

Note: 4.0g of zeolite A were used.

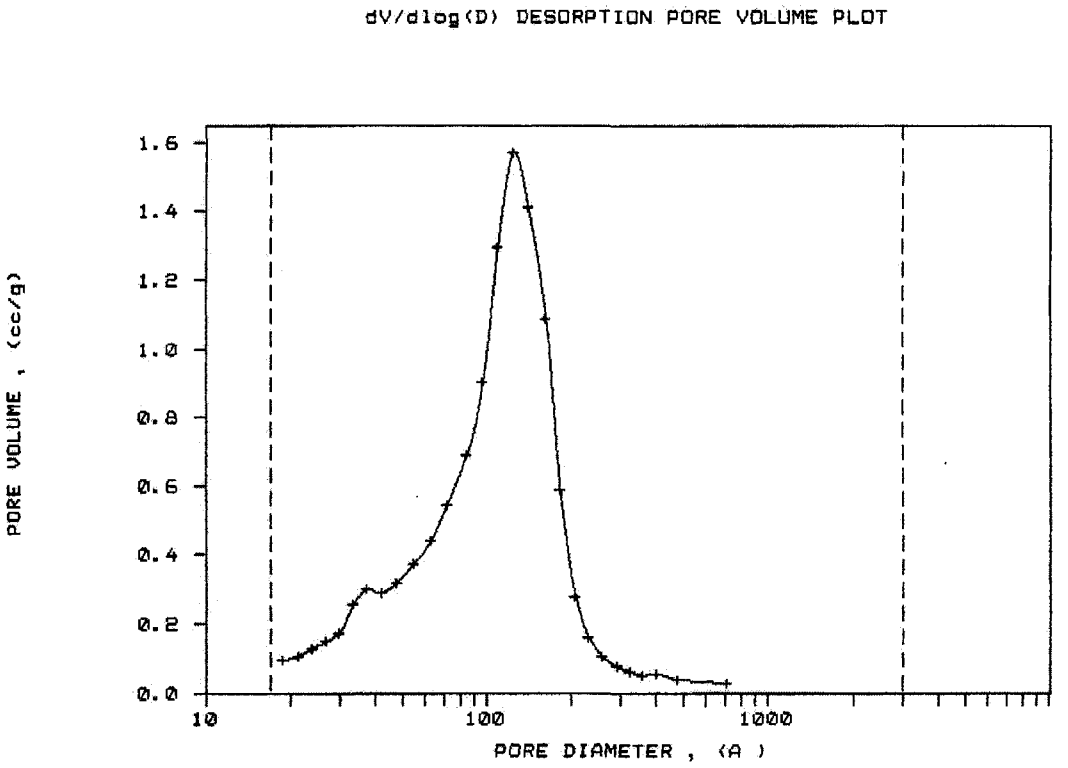


Figure 3.2 Pore size distribution for dealuminated NaA zeolite sample DeNaA-3

Under selected experimental conditions (the same as for sample DeNaA-2), reproducibility tests were conducted. Results obtained are shown in Table 3.9. It can be seen that good reproducibility are observed. For 5 runs, relative standard deviations (RSD) for surface area, pore diameter and total pore volume are 2.1%, 2.8% and 3.1%, respectively.

Table 3.9 Reproducibility test for dealumination of NaA zeolite

| Sample ID | $S_{BET}$ $m^2/g$ | $D_{av.}$ nm | $V_t$ cc/g | $V_{mic}$ cc/g | Desorption pore volume plot |
|---|---|---|---|---|---|
| DeNaA-4 | 254.1 | 10.0 | 0.64 | 0 | 1peak |
| DeNaA-5 | 255.6 | 9.7 | 0.62 | 0 | 1peak |
| DeNaA-6 | 248.1 | 10.1 | 0.63 | 0 | 1peak |
| DeNaA-7 | 249.4 | 9.5 | 0.59 | 0 | 1peak |
| DeNaA-8 | 242.5 | 10.1 | 0.61 | 0 | 1peak |

Note: 4.0g of zeolite A were used.

### 3.1.3 Dealumination of Zeolite Y and Mordenite

Le Van Mao et al. pointed out that the pore enlargement upon treatment of various A and X type zeolites with AHFS is strongly dependent on the Si/Al ratio and the preparation condition. In particular, the higher the Si/Al ratio, the lower the average size of the mesopores of the resulting materials[52]. This can be seen from our experimental results shown in sections 3.1.1 and 3.1.2. Compared with zeolite A, zeolite X has a higher Si/Al ratio and its pore enlargement is more limited than those occurring in the case for zeolite A under similar operation conditions. In this work we try to use zeolite Y and mordenite, which have higher Si/Al ratio compared with zeolites A and X (See Table 1.1), as starting materials in dealumination by AHFS treatment. Results obtained are shown in Tale 3.10, where DeLZY is used to represent the samples obtained from zeolite Y in $NH_4^+$ form, and DeM represents those from Na mordenite.

Table 3.10 Experimental results for dealuminations of Y zeolite and Na mordenite

| Sample ID | $S_{BET}$ $m^2/g$ | $D_{av.}$ nm | $V_t$ cc/g | $V_{mic}$ cc/g | Desorption pore volume plot |
|---|---|---|---|---|---|
| DeLZY-Parent | 645.5 | 1.9 | 0.34 | 0.23 | 1peak |
| DeLZY-1 AHFS:20ml Rate:1.1 ml/min RoomTem-1hr | 678.1 | 1.9 | 0.36 | 0.23 | 1peak |
| DeLZY-2 AHFS:30ml Rate:1.1 ml/min 80°C-1hr | 536.1 | 2.1 | 0.32 | 0.18 | 2peaks |
| DeLZY-3 AHFS:30ml Rate:1.1 ml/min 80°C-2hr | 361.3 | 4.0 | 0.36 | 0.10 | 2peaks |
| DeM-Parent | 359.1 | 1.6 | 0.16 | 0.13 | irregular |
| DeNaM-1 AHFS:20ml Rate:1.1 ml/min RoomTem-1hr | 279.2 | 1.7 | 0.13 | 0.10 | irregular |

Note: 4.0g of zeolites were used.

It can be seen from Table 3.10 that when zeolite Y was treated by 20 $cm^3$ of AHFS at room temperature for 1 hour (other conditions are the same as described in experimental section 2.2), the micropore volume of the resulting sample remains unchanged compared with the parent zeolite. As the volume of the AHFS solution used increased to 20 $cm^3$ and the reaction took place at 80°C for 1 hour, the micropore volume decreased from 0.13 to 0.10 $cm^3 \cdot g^{-1}$(by 23%), and correspondingly the BET surface area of the sample decreased from 359 to 279 $m^2 \cdot g^{-1}$(by 22%). Under similar operation conditions with the reaction time prolonging to 2 hours, the micropore volume decreased

by 64%, while the BET surface area of the sample decreased by 44%. It seems that in dealumination of zeolite Y by AHFS treatment, the disappearance of micropores is accompanied by pore structure collapse, and mesopore formation is rather limited. Figure 3.3 a and b show the pore size distribution for sample DeLZY-1 and DeLZY-2 (micropores have not been shown). In each plot a sharp peak and a very board peak can be observed. The occurrence of the very board peak indicated the pore structure destruction in the AHFS treatment under relatively severe condition.

Similar experimental results were obtained in using mordenite as starting material. Figure 3.3 c shows the pore size distribution for sample DeM-1. Obviously, pore enlargement technique that has been successfully used for zeolites A and X is not so effective for zeolite Y and mordenite. As discussed in introduction section1.5.5, pore size enlargement is a result of the removal of alumino-silicate "clusters" from the zeolites framework by extraction of Al atoms, which actually defined the cleavage line of the clusters. Since Si-rich zeolites can only supply less Al-cleavage points, the removal of such clusters is certainly rather difficult. These results indicate that the order of the stability against AHFS treatment is as follows:

Na mordenite > Y zeolite > NaX zeolit > Na A zeolite

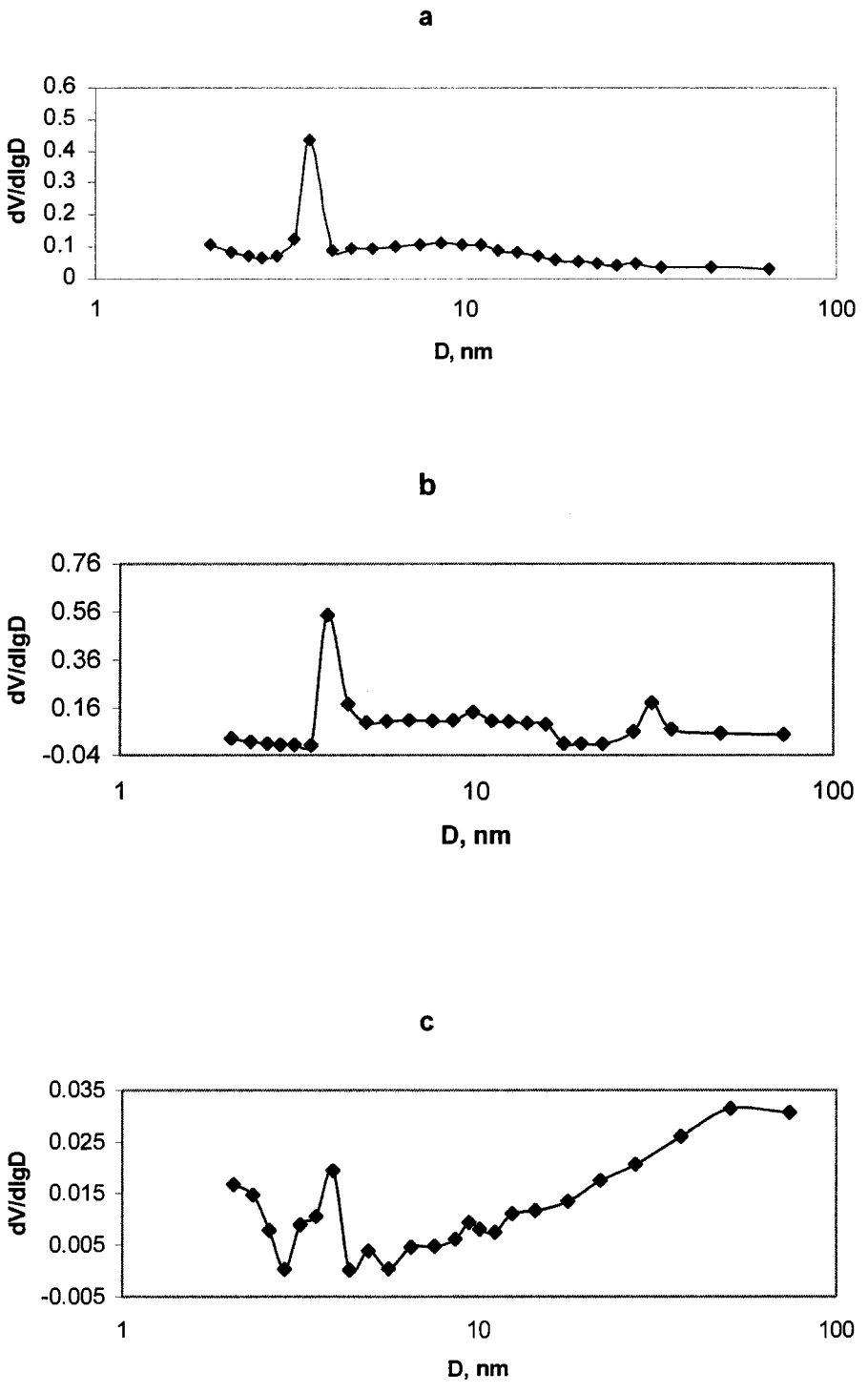


Figure 3.3 Pore size distribution for (a) DeLZY-1 (b) DeLZY-2 and (c) DeM-1

## 3.2 Characteristics of Silica Nanoboxes

### 3.2.1 Pore Shapes and Textural Properties

As can be seen from our results given above, for the 4 types of zeolites tested, only NaX and NaA zeolites can be used as starting materials for preparing mesoporous aluminosilicates by AHFS treatment. For convenience, in the following discussion, we call them nanoboxes from NaX zeolite and nanoboxes from NaA zeolite, respectively. The textural properties for the two types of nanoboxes have been characterized by nitrogen adsorption/desorption isotherm investigations. As discussed in above sections, the mesopores of nanoboxes from NaX zeolite have very narrow pore size distribution, with average pore size diameter ranging from 3.6 to 5.0 nm depending on the experimental conditions; while the mesopores of the nanoboxes from NaA zeolite also have rather narrow pore size distribution, with average pore size diameter of 11 -16 nm.

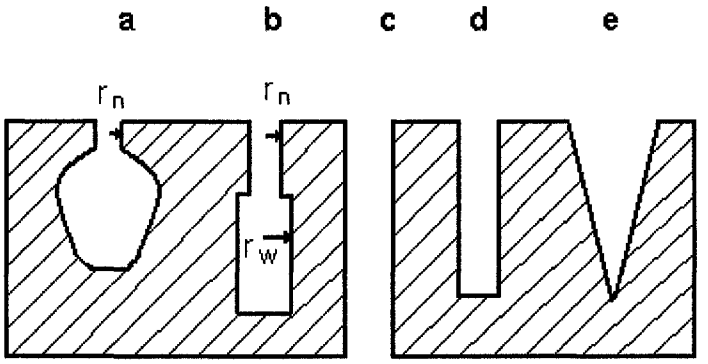


Figure 3.4 Five types of possible pore shapes for silica nanoboxes[66]

In preparation of silica nanoboxes by AHFS leaching, the possible pore shapes formed onto the zeolites matrix may be as shown in Figure 3.4. It has been discussed in refs. [66,67] that the type of hysteresis loop in nitrogen adsorption/desorption isothem may give the clue about the pore shape. For example, in case (a), the pores are of short-necked ink-bottle-shape, with a wide and sloping body, and the corresponding hysteresis loop should be similar to Type E in ref. [66]. This type of hysteresis loop is essentially composed from a sloping adsorption branch and a steep desorption branch. For case (b) the pores are of wide necked ink-bottle-shape ($r_n < r_w < 2r_n$), and the corresponding hysteresis loop should be similar to H1 in Figure1.22 or type A in ref. [66]. For case (c), the pores are essentially the cylindrical capillaries, open at both ends, and the hysteresis loop is similar to that for case (b), but the adsorption branch should be steeper than the desorption one[70], and the following equation holds[66]:

$$(p_a/p_o)^2 = p_d/p_o \qquad (3\text{-}1)$$

where $p_a/p_o$ and $p_d/p_o$ are reduced pressures corresponding to the steep parts on adsorption and desorption branches, respectively. Finally, in cases of (d) and (e), no hysteresis loop is observed.

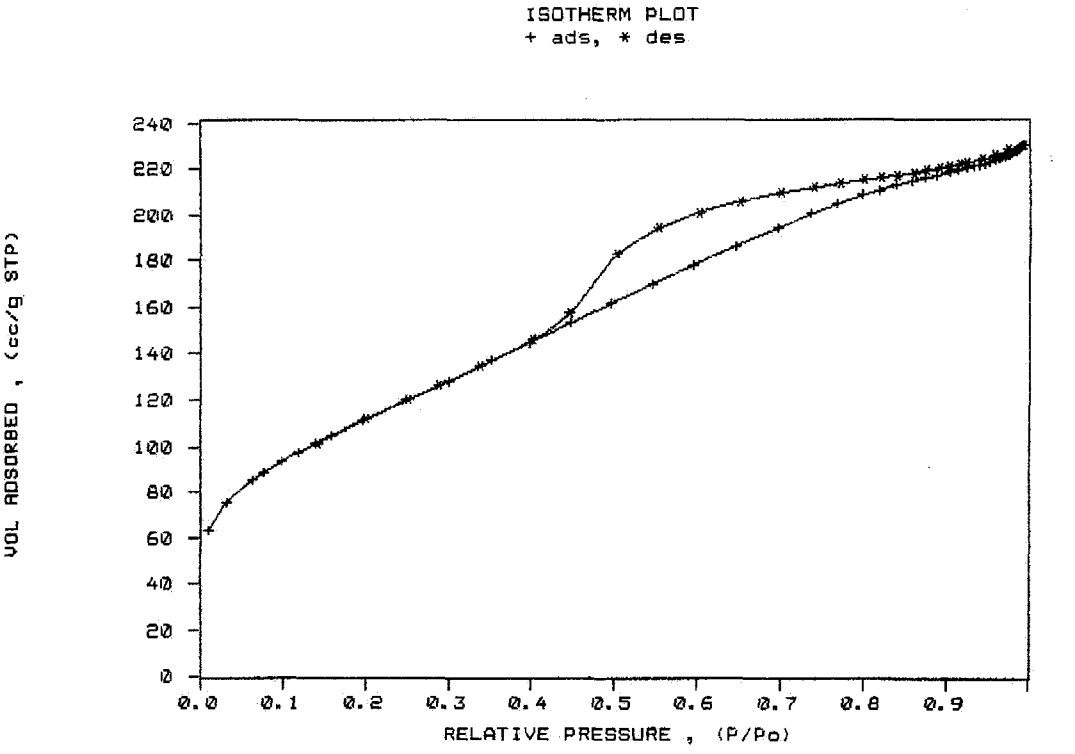


Figure 3.5 Hysteresis loop for silica nanoboxes from NaX zeolite

In fact, the hysteresis loop for nanoboxes from zeolite NaX (typically as given in Figure 3.5) is similar to Type E in ref. [66]. This strongly suggests that the mesopores obtained by AHFS treatment in this case are ink-bottle-shape capillaries with short necks and wide, sloping bodies (shape group XIV in ref. [66], as shown in Figure 3.4-a). However, the steep part on desorption branch in our case is not so steep. This may be due to the irregular cross section of the short necks (or/and with nonuniform radii).

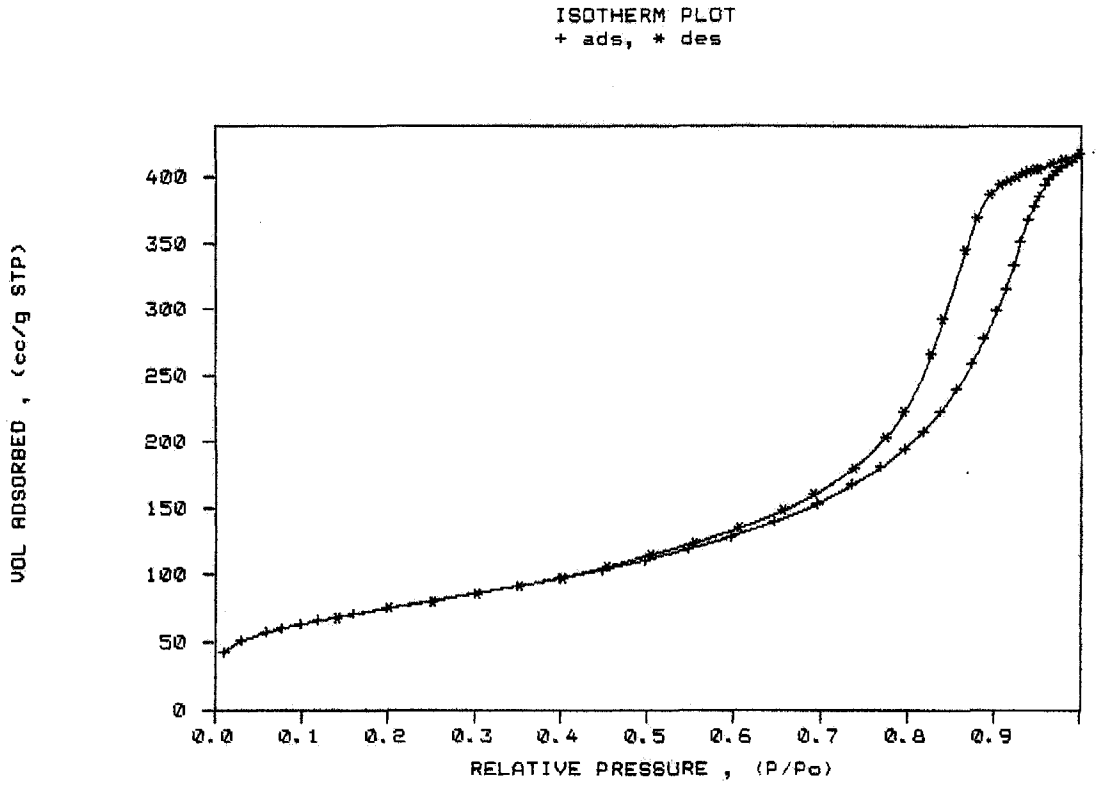


Figure 3.6 Hysteresis loop for silica nanoboxes from NaA zeolite

The hysteresis loop for nanoboxes from zeolite NaA (See Figure 3.6) is similar to H1 in Figure 1.22 and type A hysteresis loop in ref. [66]. This shape group may be attributed to cylindrical pores with open ends, or wide necked ink-bottled-shaped one. Considering the more sloping adsorption branch and a narrower hysteresis loop, it is more likely that the mesopores formed by AHFS treatment in this case are wide necked ink-bottle-shaped capillaries (See ref. [66] shape group IV, as shown in Figure 3.4-b). It is worth to note that the two steep parts on both adsorption and desorption branches are sloping. These may be due to the nonuniform dimensions of the mesopores.

Some of the textural properties of nanoboxes from zeolites NaX and NaA are given in Table 3.11.

Table 3.11 Textural properties of nanoboxes from NaA and NaX zeolites

| Sample ID | $S_{BET}$ $m^2/g$ | $D_{av.}$ nm | $V_t$ cc/g | $V_{mic}$ cc/g | Desorption pore volume plot |
|---|---|---|---|---|---|
| NaX Parent zeolite | 867 | 1.5 | 0.35 | 0.33 | 3 peaks |
| DeNaX | 361 | 3.8 | 0.34 | 0 | 1 peak |
| NaA Parent zeolite | - | (4) | - | - | Several peaks |
| DeNaA | 201 | 14.5 | 0.73 | 0 | 1 peak |

Note: Preparation conditions for DeNaA are the same as for DeNaA-3, and for De NaX are the same for DeNaX-2; Nitrogen does not significantly adsorbed by zeolite NaA. Data in brackets are estimated based on information from other sources.

### 3.2.2 Thermal and Hydrothermal Stability of Silica Nanoboxes From NaX

Thermal stability is one of the most important properties for solid catalysts and catalyst supports. Results of TGA and DTA for H form nanoboxes from zeolite X (H-DeX) and for the same material loading 15 wt% of TFA are shown in Figures 3.7 and 3.8, respectively. It can be seen from Figures 3.7 that at lower than 300°C, with increasing temperature, the moisture adsorbed is removed gradually, and within the whole tested temperature range not other significant change is observed. However, Figure 3.8 indicates that at lower than 300°C, with increasing temperature, the moisture and part of TFA (b.p. = 163°C) adsorbed are removed. It is possibly that at about 300°C, TFA chemically

bound on the surface of the dealuminated zeolite and shows a positive peak in DTA diagram. This implies that only a very small part of TFA (estimated to be 5%) can be chemically adsorbed on the dealuminated zeolite surface.

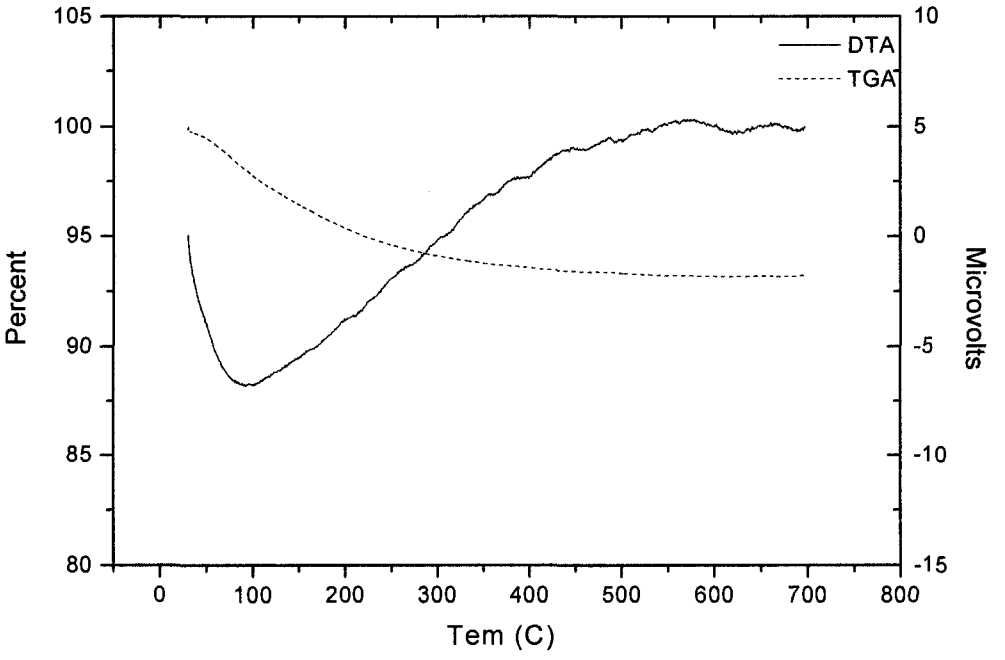


Figure 3.7 TGA and DTA results for H-DeX

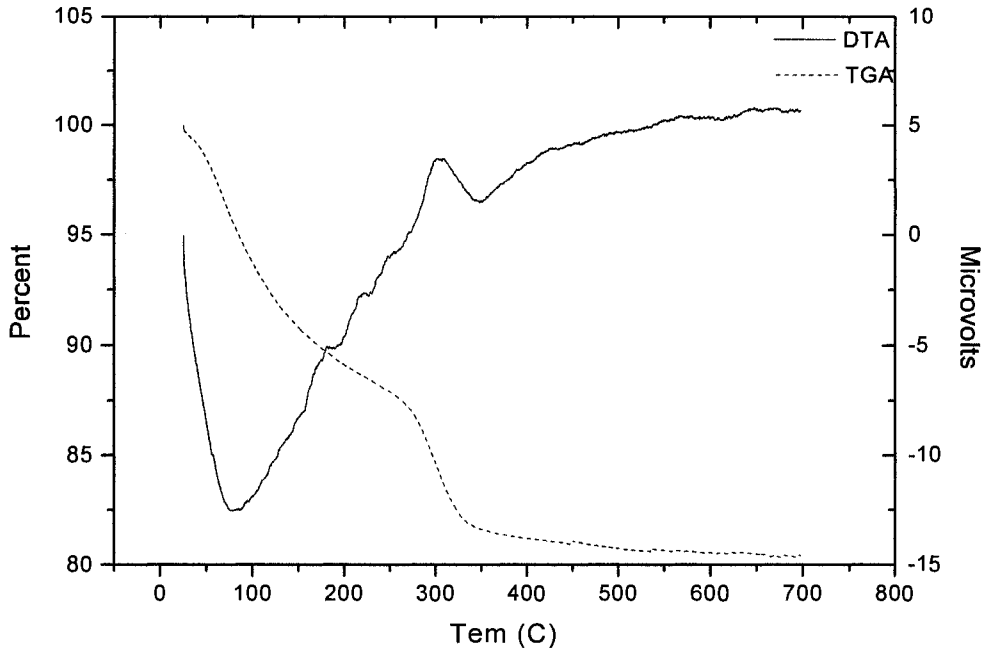


Figure 3.8 TGA and DTA results for H-DeX loading 15% of TFA

Generally speaking, silica nanoboxes prepared from pore enlargement by AHFS have better thermal stability, as have been proven by TGA/DTA investigation in previous work[52]. However, thermal stabilities of the pore enlargement products actually depend on many factors. We have found that in some cases micropores may be present in the product after AHFS treatment (bimodal nanoboxes), and in these case low thermal stability will be observed. As these micropores have been eliminated (monomodal nanoboxes), thermal stability may become much higher. As shown in Table 3.19, DeNaX(m)1 is a sample monomodal silica nanoboxes, and after calcinations at 700°C for 3 hours, its BET surface area decreases from 392 to 280 $m^2 \cdot g^{-1}$; while DeNaX(b)1 is a sample of bimodal silica nanoboxes, and it seems that its porous structures have been

severely destroyed after calcination. DeNaX(m)2 is also a sample of monomodal nanoboxes, which was prepared by treating 2 g of DeNaX(b)1 with 50 $cm^3$ of 0.04 $mol \cdot dm^{-3}$ HCl for 1 h to eliminate the micropores. Obviously, compared with DeNaX(b)1, thermal stability for DeNaX(m)2 has been significantly improved by this treatment (See Table 3.12).

Table 3.12 Changes in textural properties of the mesoporous products before and after calcination

| Sample ID | $S_{BET}$ $m^2/g$ | $D_{av.}$ nm | $V_t$ cc/g | $V_{mic}$ cc/g | Desorption pore volume plot |
|---|---|---|---|---|---|
| DeNaX(m)-1 before calcination | 392 | 4.4 | 0.43 | 0 | 1 peak |
| DeNaX(m)-1 after calcination at 700°C for 3h | 280 | 4.8 | 0.33 | 0 | 1 peak |
| DeNaX(b)-1 before calcination | 340 | 3.1 | 0.26 | 0.01 | 1 peak |
| DeNaX(b)-1 after calcination at 700°C for 3h | 5.8 | 8.6 | 0.01 | 0 | Several peaks |
| DeNaX(m)-2 before calcination | 319 | 3.6 | 0.26 | 0 | 1 peak |
| DeNaX(m)-2 after calcination at 700°C for 3h | 176 | 4.2 | 0.19 | 0 | 1 peak |

For materials used as catalysts or catalyst supports, their hydrothermal stabilities are one of key factors to be considered. In the present work hydrothermal stability tests are conducted and the results are given in Table 3.13.

It can be seen that as the silica nanoboxes from zeolite NaX (sample DeNaX) was calcined at 300°C for 3 hours and then at 600°C for 3 hours, the surface area changed from 361 to 222 $m^2 \cdot g^{-1}$ (sample DeNaX-c), decreased by 38.5%. At the same time, the average pore diameter increased from 3.8 to 4.8 nm. Similar to other kinds of zeolite products, the first calcination may result in a surface area decrease to some extent. It seems that calcinations did not severely damage the framework of the silica nanoboxes in this case. After mixing with 20 wt% Bentonite (sample DeNaX-e), the surface area showed a slightly decrease (from 222 to 181 $m^2/g$). Finally, the sample was calcined at 600°C for 3 hours and underwent hydrothermal treatment (sample DeNaX-h, number 1 and 2 denote the two repeated experiments). After that the surface area only decreased by 12%. This implies that sample DeNaX has satisfactory hydrothermal stability, though hydrothermal treatment may result in changing the pore size distribution to a slight degree.

Table 3.13 Hydrothermal stability test for Na-form silica nanoboxes from X zeolite

| Sample ID | $S_{BET}$ $m^2/g$ | $D_{av.}$ nm | $V_t$ cc/g | $V_{mic}$ cc/g | Desorption pore volume plot |
|---|---|---|---|---|---|
| DeNaX | 361.1 | 3.8 | 0.34 | 0 | 1peak |
| DeNaX-c | 221.6 | 4.8 | 0.27 | 0 | 1peak |
| DeNaX-e | 180.6 | 5.1 | 0.23 | 0 | 1peak |
| DeNaX-h1 | 159.3 | 5.5 | 0.21 | 0 | 1peak with a shoulder |
| DeNaX-h2 | 162.1 | 5.6 | 0.23 | 0 | 1peak with a shoulder |

A hydrothermal stability test for the acid form of silica nanoboxes from NaX zeolite has also been performed in the same way as described above. Similar results are observed as given in Table 3.14. Sample codes are similar to those shown in Table 3.13.

Table 3.14 Hydrothermal stability test for acid form of silica nanoboxes from X zeolite

| Sample ID | $S_{BET}$ $m^2/g$ | $D_{av.}$ nm | $V_t$ cc/g | $V_{mic}$ cc/g | Desorption pore volume plot |
|---|---|---|---|---|---|
| $DeNH_4X$ | 317.1 | 3.8 | 0.39 | 0 | 1peak |
| H-DeX-c | 243.3 | 4.3 | 0.32 | 0 | 1peak |
| H-DeX-e | 192.5 | 5.5 | 0.27 | 0 | 1peak |
| H-DeX-h1 | 180.6 | 5.6 | 0.25 | 0 | 1peak with a shoulder |
| H-DeX-h2 | 176.3 | 5.7 | 0.25 | 0 | 1peak with a shoulder |

### 3.2.3 Physicochemical Properties of Silica Nanoboxes from NaX

Si/Al ratio and degrees of crystallinity are two important physicochemical properties for zeolites and the related products. Table 3.15 shows the Si/Al ratio determined by atomic absorption spectroscopy for two forms of silica nanoboxes and their parent zeolite. In our laboratory, similar work has been done previously[63]. For comparison, the corresponding data are also given in the Table 3.15. Two sets of experimental results are essentially consistent with each other. Based on $^{29}Si$ MAS NMR

spectrum of DeNaX the Si/Al value is estimated to be 3.5[63]. These indicate that by carefully controlling experimental conditions so as to fulfill certain requirements, we can obtain the silica nanoboxes of desired properties with rather high reproducibility.

In fact, pore size enlargement is a result of the removal of alumino-silicate "clusters" from the zeolite framework by extraction of Al atoms, and consequently, the degrees of crystallinity of the resulting product may decrease. Crystallinity data shown in Table 3.15 are also cited from previous works conducted in our laboratory. As shown in the table, after AHFS treatment, a significant increase in Si/Al ratio and lower degrees of crystallinity of the dealuminated products can be observed compared with their parent zeolite. Lower content of Al means lower ion-exchange capacity, and higher Si/Al ratio means higher hydrophobicity. Though the dealuminated product exhibits low crystallinity, a study by X-ray powder diffraction at very small angles clearly shows the periodicity of these nanoboxes throughout the mesoporous material[65].

Table 3.15 Si/Al ratio and degree of crystalliniy for parant zeolite and silica nanoboxes from zeolite NaX

| Sample ID | Si/Al (atom ratio) | | degree of crystallinity |
|---|---|---|---|
| | Present work | Previous work[69] | % |
| NaX Parent zeolite | 1.2 | 1.2 | 100[58] |
| DeNaX | 2.8 | 3.2 | <40[58] |
| H-DeX | 3.2 | 3.9 | low[69] |

Ion-exchange capacity (IEC) is another important physicochemical property for the above materials. According to the chemical composition data for NaX zeolite (Linde,

Si/Al ratio = 1.22, $Na_2O\%$ = 20.5) given in ref. [58], IEC is estimated to be 6.62 mmol/g zeolite. However, our determination result indicates that IEC for H form nanoboxes from NaX zeolite is 3.87 mmol/g zeolite. This implies that silica nanoboxes exhibit much lower ion-exchange capacity than their parent zeolite.

### 3.3 Dehydration of Ethanol over Different Catalysts

Five catalysts (H-DeX-15%-TFA, H-DeX, H-ZSM-5/50, H-USY and HY zeolites) have been used in catalytic dehydration of ethanol at reaction temperature of 200°C with weight hourly space velocity (WHSV) of 1 $h^{-1}$. The aqueous ethanol concentration is 20 wt%. The total conversion of ethanol and the selectivity to products are given in Table 3.16.

Table 3.16 Catalytic activity of ethanol dehydration over different catalysts

| Catalyst Type | Total Conversion | Product Selectivity % | | | | | | Yield of Hydrocarbons |
|---|---|---|---|---|---|---|---|---|
| | % | Ethylene | Propylene | Diethyl Ether | $C_{1-6}$ | $C_{4-6}^{=}$ | Aromatics | % |
| HZSM-5/50 (a) | 57 | 41 | 0 | 59 | 0 | 0 | 0 | 23.1 |
| HY | 47 | 11 | 0 | 89 | 0 | 0 | 0 | 5.4 |
| H-USY | 40 | 10 | 0 | 88 | 2 | 0 | 0 | 4.8 |
| H-DeX - 15%TFA (b) | 28 | 23 | 0 | 75 | 1 | 0 | 0 | 6.7 |
| H-DeX | 11 | 40 | 0 | 58 | 2 | 0 | 0 | 4.6 |

a. Number 50 in this case is used to represent the ratio of $SiO_2/Al_2O_3$.

b. TFA loading on H-DeX

In this study, ethanol-to-hydrocarbons or ETH can be seen as the measurement of catalytic activity of the catalyst. The yield of hydrocarbons is defined as the total conversion of ethanol multiply by its product selectivity. Since ethylene is the primary product of ethanol dehydration, the yield of ethylene could be also used to measure the catalytic performance in most cases. The results from Table 3.16 indicate that the order of catalytic activity to hydrocarbons of the catalysts is:

H-ZSM-5/50 > H-DeX-15%-TFA > H-Y > H-USY> H-DeX

This order can be explained by their surface acidity (density and strength). See Table 3.17 for the total surface acidity of each catalyst.

Table 3.17 Total acidity by $NH_3$-TPD/ISE method

| Type of Catalyst | $SiO_2/Al_2O_3$ Ratio | Calculated [Al] Concentration (mmol/gcat.) | Acid Sites Density Determined by ISE (mmol/gcat.) |
|---|---|---|---|
| H-ZSM-5/50* | 50 | 0.546 | 0.488 |
| HY* | 6.28 | 4.021 | 3.45 |
| H-USY* | 5.47 | 4.463 | 1.58 |
| H-DeX | 6.4 | 3.97 | 1.15 |

Note: * indicates data from ref.[68]

It can be seen that for H-Y, H-USY and H-DeX, the order of catalytic activity is in accord with their acid site densities. Although a high amount of TFA (15 wt%) incorporated with H-DeX results increasing on the catalytic activity among those faujasite type zeolite catalysts, especially increasing on the selectivity to light olefins, but

the catalytic activity is still much lower when compared to H-ZSM-5 zeolite catalyst. This result does not agree with our previous expectation. The reason could be that the absorption of TFA on the surface of those silica nanoboxes (H-DeX) is not chemically as strong as expected[10]. Surprisingly, H-ZSM-5/50 has a much higher activity than catalysts mentioned above even though its acid site density is not so high. However, this can be explained by the higher strength of its acid sites. Figure 3.9 shows the strength of acid sites distribution. It can be seen that for H-ZSM-5/50, the strong acid sites from which $NH_3$ could be desorbed at temperature greater than 450°C is much stronger than that from HY or H-USY. Therefore, it is suggested that those strong acid sites should be the active sites for the dehydration of ethanol.

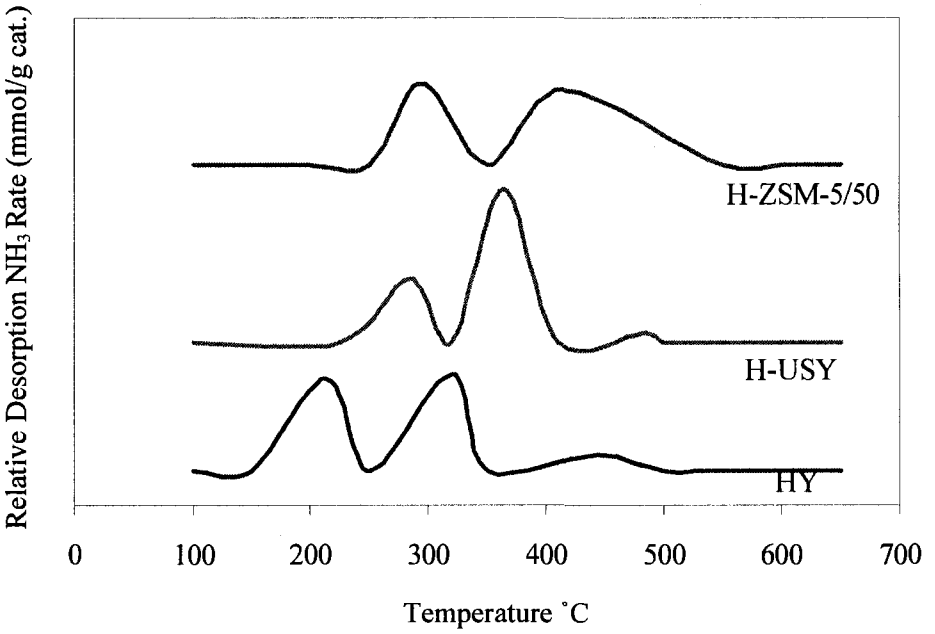


Figure 3.9Acidity profile (strength) by $NH_3$-TPD/ISE[62]

### 3.4 Effect of $SiO_2/Al_2O_3$ Ratio on Ethanol Dehydration

For ZSM-5 family, the effect of $Si_2/Al_2O_3$ ratio on catalytic activity has been studied at 200°C with weight hourly space velocity (WHSV) of 1 $h^{-1}$. The aqueous ethanol concentration is 20 wt%. The results show that the catalytic activity decreases as the $SiO_2/Al_2O_3$ ratio increase. Experimental results are given in Table 3.18.

Table 3.18 Catalytic activity for H-ZSM-5 with different $SiO_2/Al_2O_3$ ratio

| $SiO_2/Al_2O_3$ | Total Conversion | Product Selectivity % | | | | | | Yield of Hydrocarbons |
|---|---|---|---|---|---|---|---|---|
| | % | Ethylene | Propylene | Diethyl Ether | $C_{1-6}$ | $C_{4-6}^{=}$ | Aromatics | % |
| 25 | 59 | 37 | 0 | 63 | 0 | 0 | 0 | 22 |
| 50 | 57 | 41 | 0 | 59 | 0 | 0 | 0 | 23 |
| 100 | 51 | 17 | 0 | 81 | 2 | 0 | 0 | 10 |
| 400 | 13 | 15 | 0 | 80 | 5 | 0 | 0 | 3 |
| 1000 | 5 | 41 | 0 | 52 | 7 | 0 | 0 | 2 |

For H-ZSM-5 series, with increasing $SiO_2/Al_2O_3$ ratio, the acid site density becomes lower and lower, the activity accordingly decreases. This can be the same explanation as section 3.3. Though H-ZSM-5/25 and H-ZSM-5/50 have nearly the same activity, but the latter has higher ethylene selectivity, and so H-ZSM-5/50 may be a more suitable catalyst for ethanol dehydration forming ethylene compared with other catalysts used. Figure 3.10 shows the dependence of yield of ethylene on $SiO_2/Al_2O_3$ ratio for H-ZSM-5 series.

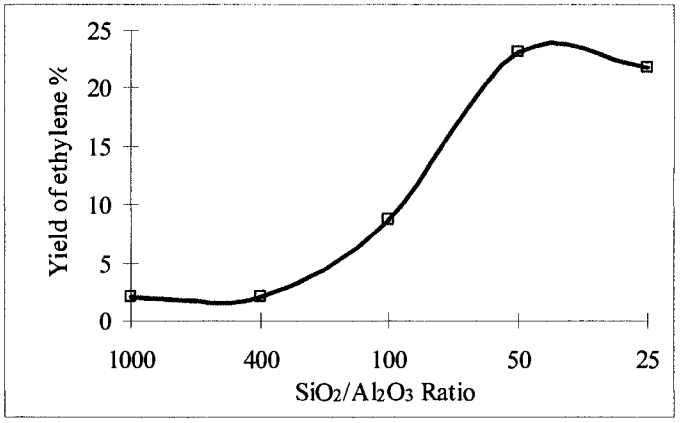


Figure 3.10 Dependence of ethylene yield on $SiO_2/Al_2O_3$ ratio for H-ZSM-5 series

### 3.5 Effect of Weight Hourly Space Velocity on Ethanol Dehydration

Using H-ZSM-5/50 as a catalyst, under given conditions (the reaction temperature is 225°C, the aqueous ethanol concentration is 60 wt%), influence of WHSV on the conversion of ethanol and the selectivity of products was investigated. Experimental results are given in Table 3.19.

Table 3.19 Effect of space velocity on catalytic activity over H-ZSM-5/50

| WSHV | Contact time | Total Conversion | Product Selectivity % | | | | | | Yield of Hydrocarbons |
|---|---|---|---|---|---|---|---|---|---|
| $h^{-1}$ | h | % | Ethylene | Propylene | Diethyl Ether | $C_{1-6}$ | $C_{4-6}^{=}$ | Aromatics | % |
| 1 | 1.00 | 98 | 97 | 0 | 1 | 0 | 1 | 0 | 97 |
| 1.5 | 0.67 | 84 | 79 | 0 | 21 | 0 | 0 | 0 | 66 |
| 2 | 0.50 | 77 | 43 | 0 | 57 | 0 | 0 | 0 | 33 |
| 3 | 0.33 | 73 | 33 | 0 | 67 | 0 | 0 | 0 | 24 |
| 4 | 0.25 | 68 | 31 | 0 | 69 | 0 | 0 | 0 | 21 |
| 5 | 0.20 | 66 | 26 | 0 | 74 | 0 | 0 | 0 | 17 |

The exact mechanism of the ethanol catalytic dehydration process is unclear, but the crucial step can be thought of as an acid-base reaction. One way to break up ethanol is to give a base - the hydroxy, $OH^-$ ion and an acid - the ethyl carbenium ion, $CH_3CH_2^+$. Strongly acid sites in the pores of the zeolite attack the OH substituent of ethanol, giving a water molecule bound to the surface and an ethyl carbenium ion.

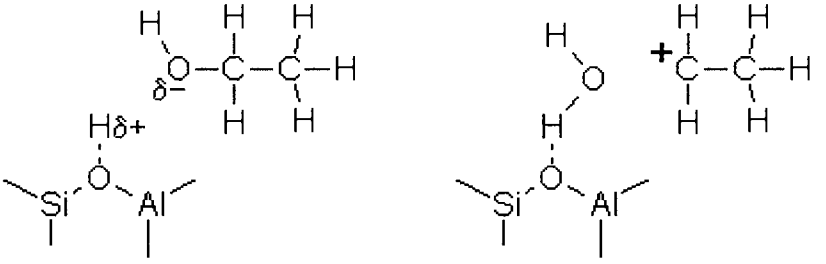

Attack of the highly acid zeolite sites gives both water and a positively charged carbon-centred ion. The $\delta^+$ and $\delta^-$ refer to sites that are a partially positive or negative.

Though this ion is highly reactive and cannot survive long in the presence of water, in the restricted environment of the zeolite pores, ethyl carbenium ion finds it is easier to lose a hydrogen ion, giving ethylene.

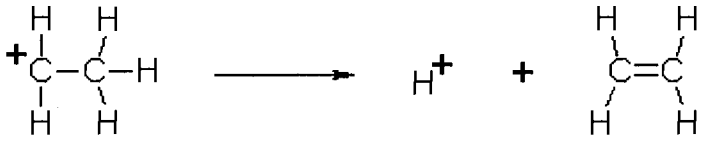

Loss of a proton

It can be seen from Table 3.19 that the main products in these cases are ethylene and diethyl ether. This implies that two reaction pathways may be involved in the dehydration of ethanol over H-ZSM-5 catalyst:

1. Direct dehydration (intramolecular dehydration)

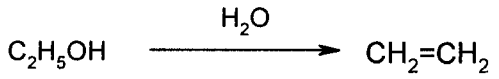


2. Indirect dehydration (intermolecular dehydration)

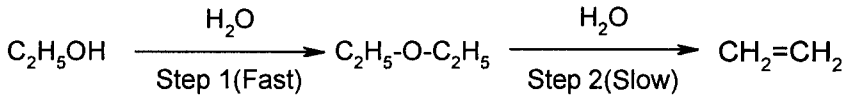


With increasing WHSV, conversion of ethanol decreases; at the same time, the ethylene selectivity decreases and the diethyl ether selectivity increases. As we know, higher WHSV is corresponding to shorter contact time, and this certainly reduces the conversion. Selectivity results shown in Table 3.19 indicate that step 1 in indirect dehydration is faster than step 2. Under the condition of short contact time (WHSV = 5 $h^{-1}$) diethyl ether is dominant in the products. Of course prolonging contact time is beneficial to the transformation of diethyl ether to ethylene.

### 3.6 Effect of Reaction Temperature on Ethanol Dehydration

H-ZSM-5/50 was used to study the effect of reaction temperature on the catalytic activity. The total conversion of ethanol and the product distribution are given in Table 3.20 (WHSV is 1 $h^{-1}$; Aqueous ethanol concentration is 20 wt%).

Table 3.20 Effect of reaction temperature on ethanol dehydration over H-ZSM-5/50

| Reaction Temperature | Total Conversion | Product Selectivity % | | | | | | Yield of Hydrocarbons |
|---|---|---|---|---|---|---|---|---|
| °C | % | Ethylene | Propylene | Diethyl Ether | $C_{1-6}$ | $C_{4-6}^{=}$ | Aromatics | % |
| 150 | 26 | 2 | 0 | 98 | 0 | 0 | 0 | 1 |
| 175 | 52 | 10 | 0 | 90 | 1 | 0 | 0 | 5 |
| 200 | 57 | 41 | 0 | 58 | 0 | 0 | 0 | 23 |
| 225 | 82 | 93 | 0 | 6 | 1 | 0 | 0 | 77 |
| 250 | 98 | 79 | 6 | 0 | 6 | 9 | 0 | 98 |
| 275 | 100 | 35 | 22 | 0 | 6 | 30 | 7 | 100 |
| 300 | 100 | 10 | 37 | 0 | 15 | 21 | 17 | 100 |
| 325 | 100 | 7 | 37 | 0 | 16 | 19 | 20 | 100 |
| 350 | 100 | 7 | 34 | 0 | 17 | 14 | 29 | 100 |

It can be seen that as the reaction temperature rises from 150°C to 350°C, the ethanol conversion increases from 26% to 100%. According to Arrhenius equation:

$$\ln k = -Ea/RT + A \quad \ln k = -Ea/RT + A \qquad (3\text{-}2)$$

where k, Ea, R, T and A are rate constant, activation energy, universal gas constant, Kelvin temperature and a constant, respectively. That is, high reaction

temperature may result in a higher rate constant. Figure 3.11 demonstrates a clear relationship between the yield of hydrocarbons and temperature. When temperature increases, more ethanol can be involved into reaction, thus, the yield of hydrocarbons increases. However, when temperature is high enough (≥250°C), the yield of hydrocarbons reaches the maximum value 100% and will not change any more.

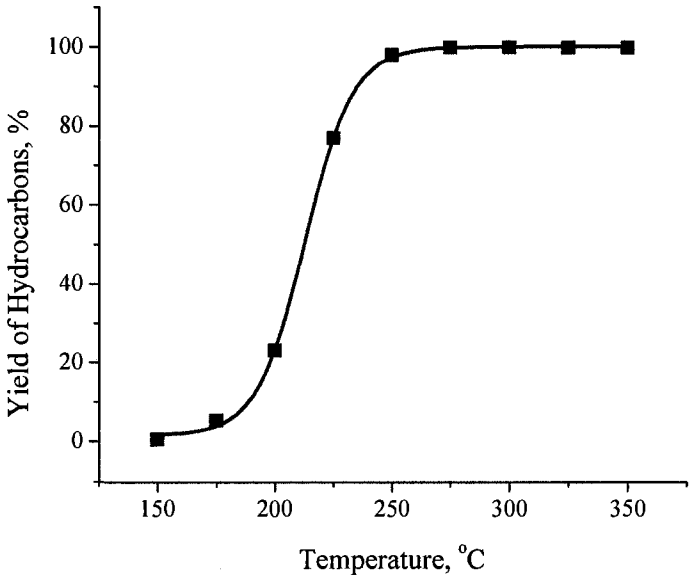


Figure 3.11 Yield of hydrocarbons vs. temperature

At 150°C diethyl ether selectivity is as high as 98%, but it reduces very rapidly as rising reaction temperature. On the other hand, with increasing reaction temperature ethylene selectivity reaches a maximum (93%) at 225°C. These results confirm that the dehydration of ethanol undergoes the two steps reaction mechanism as mentioned in section 3.5, ethylene is produced through the formation of diethyl ether as a reaction intermediate. Low temperature is favourable for the formation of diethyl ether and high

temperature is suitable for the production of ethylene. In recent years, many researchers consider the "hydrocarbon pool" mechanism for the olefinic production. However, our results do not suggest this mechanism due to the low reaction temperature. A higher production of propylene should be observed if it is a case of the hydrocarbon pool mechanism.

At temperatures higher than 250°C, many secondary reactions such as oligomerization plus cracking, metathesis and aromatization etc. may take place, therefore, the ethylene selectivity decreases, meanwhile, the propylene selectivity and other hydrocarbons ($C_1$- $C_6$ paraffins, $C_4^=$-$C_6^=$ olefins, and BTX Aromatics) selectivity increase. The propylene selectivity has a maximum (37%) at 325°C.

At 275°C, the selectivity to ethylene plus propylene reaches the maximum (57%); this indicates that 275°C is the best reaction temperature to produce ethylene plus propylene. Figure 3.12 shows the dependence of product selectivity on reaction temperature.

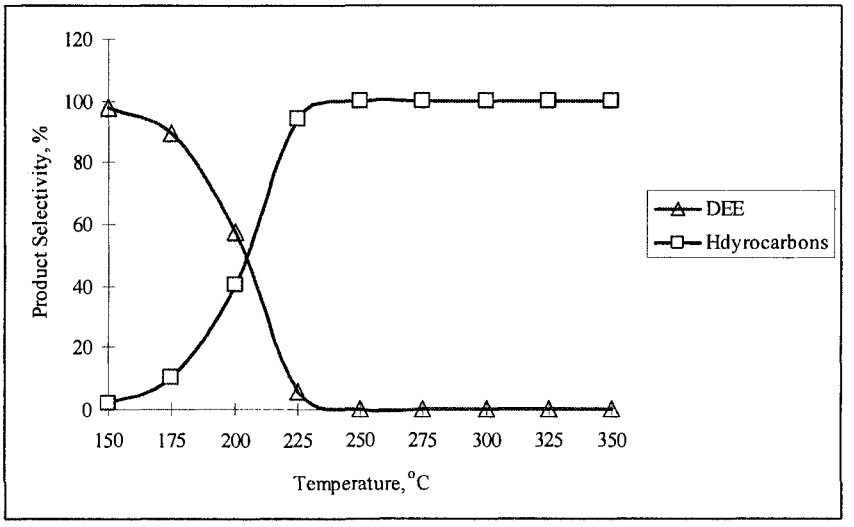


(a)

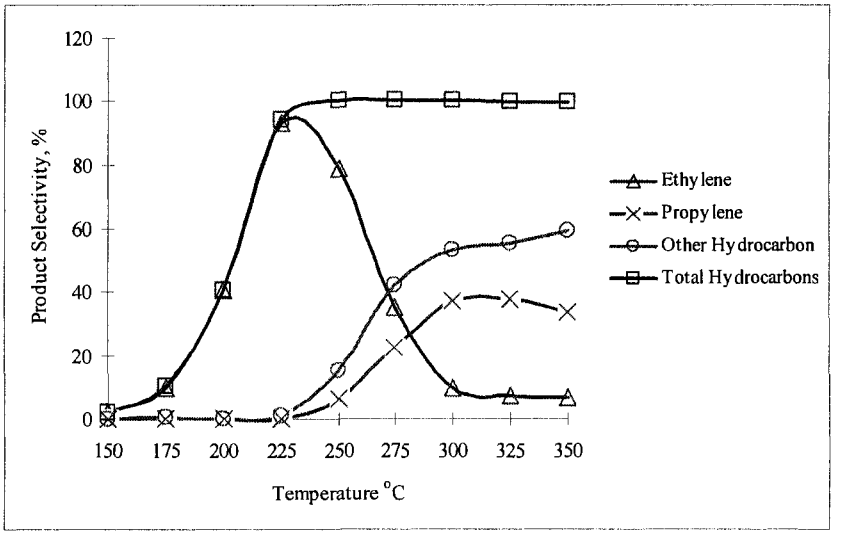


(b)

Figure 3.12 Dependence of product selectivity on reaction temperature

A series of testing was carried out at 275°C using catalyst H-ZSM-5 with $SiO_2/Al_2O_3$ ratio of 25, 50 and 100, also fluorinated H-ZSM-5. The total conversion and the product selectivity are given in Table 3.21(WSHV is 1 $h^{-1}$; Aqueous ethanol concentration is 20 wt%). The results show that the yield of hydrocarbons from different $SiO_2/Al_2O_3$ ratio HZSM-5 catalysts has the same value(100%), but the product distribution are vary, the selectivity to ethylene increases from 21% to 91% with the $SiO_2/Al_2O_3$ ratio from 25 to 100, meanwhile, the selectivity to ethylene also increases when H-ZSM-5 zeolite is fluorinated. Therefore, the desirable light olefinic product can be selectively produced by using modified H-ZSM-5 zeolite catalysts.

Table 3.21 Catalytic activity and product selectivity over H-ZSM-5 and fluorinated H-ZSM-5

| Catalyst Type | Total Conversion | Product Selectivity % | | | | | | Yield of Hydrocarbons |
|---|---|---|---|---|---|---|---|---|
| | % | Ethylene | Propylene | Diethyl Ether | $C_{1-6}$ | $C_{4-6}^{=}$ | Aromatics | % |
| HZMS-5/25 | 99 | 21 | 29 | 0 | 8 | 36 | 7 | 100 |
| HZMS-5/50 | 99 | 35 | 22 | 0 | 6 | 30 | 7 | 100 |
| HZMS-5/100 | 99 | 93 | 3 | 0 | 1 | 2 | 1 | 100 |
| HZMS-5/25F3 | 99 | 23 | 25 | 0 | 9 | 36 | 7 | 100 |
| HZMS-5/50F3 | 99 | 91 | 4 | 0 | 0 | 4 | 1 | 100 |

Note: HZSM-5/25F3 and HZSM-5/50F3 indicate 3.5 wt% of $NH_4F$ loaded on HZSM-5 zeolite

### 3.7 Effect of Aqueous Ethanol Concentration on Ethanol Dehydration

The effects of aqueous ethanol concentration on ethanol dehydration are shown in Table 3.22. It can be seen that under given conditions (reaction temperature is 225°C, WSHV is 1 $h^{-1}$, catalyst is H-ZSM-5/50), with increasing aqueous ethanol concentration from 20% to 99%, ethanol conversion increases from 82% to 99%, meanwhile, the yield of hydrocarbons increases from 77% to 98%. In our case no significant effect on the product distribution was observed.

Table 3.22 Effect of aqueous ethanol concentration on the ethanol dehydration over H-ZSM-5/50

| Aqueous ethanol concentration | Total Conversion | Product Selectivity % | | | | | | Yield of Hydrocarbons |
|---|---|---|---|---|---|---|---|---|
| wt% | % | Ethylene | Propylene | Diethyl Ether | $C_{1-6}$ | $C_{4-6}^{=}$ | Aromatics | % |
| 20 | 82 | 93 | 0 | 6 | 1 | 0 | 0 | 77 |
| 40 | 84 | 95 | 0 | 4 | 0 | 0 | 0 | 80 |
| 60 | 98 | 97 | 0 | 1 | 0 | 1 | 0 | 96 |
| 80 | 100 | 96 | 1 | 1 | 1 | 1 | 0 | 99 |
| 99 | 100 | 96 | 0 | 1 | 1 | 1 | 0 | 98 |

Obviously, changing aqueous ethanol concentration is corresponding to change the initial concentration of ethanol and the water content in the catalytic system. These results can be explained by the competition between ethanol and water molecules

adsorbed on the acid sites on the zeolites surface. High concentration of ethanol means low concentration of water, therefore, more ethanol molecules can be adsorbed on the acid sites, and ethanol molecules have better chance to convert into hydrocarbons.

# Chapter 4 Conclusion

The goals of this work are to investigate the best catalyst and reaction conditions for the production of hydrocarbons mainly ethylene and/or propylene from aqueous ethanol. Meanwhile, the preparation of silica nanoboxes from zeolites by dealumination based on AHFS treatment, characterization the obtaining products and their catalytic behaviors in the dehydration of ethanol were also studied. After a series of investigations, our achievements can be summarized as follows:

Silica nanoboxes prepared by AHFS treatment from zeolite X at elevated temperatures ranging from 50 to 70°C have a rather narrow pore size distribution, with average pore size diameter of 3.6 - 5.0 nm, and are of ink-bottle-shaped capillaries with short necks and wide, sloping bodies. Influence of operation conditions on the textural properties were investigated in detailed.

Silica nanoboxes from zeolite A by AHFS treatment also have a narrow pore size distribution, with average pore size diameter ranging from 11 to 16 nm, and are wide necked ink-bottle-shaped capillaries.

Preliminary experiments were conducted using zeolite Y (in $NH_4^+$ form) and Na mordenite as starting materials, respectively, with the intension of preparing silica nanoboxes by AHFS treatment. It has been found that pore enlargement technique mentioned above is not so effective for zeolite Y and mordenite.

Under selected experimental conditions, silica nanoboxes from zeolite NaA and from zeolite NaX (DeNaA and DeNaX) were prepared and were characterized by using

nitrogen adsorption/desorption isotherm investigations, atomic adsorption spectrophtometry, combined thermogravimetric and differential thermal analyses. Their high chemical and thermal stabilities as well as the special pore features suggest that these mesopororous materials have potential advantages in practical applications.

Different type of acidic form zeolite catalysts such as H-DeX, H-DeX -15% TFA, H-USY, H-Y and H-ZSM-5 have been used in catalytic dehydration of ethanol at 200°C with weight hourly space velocity (WHSV) of 1 $h^{-1}$. The order of catalytic activity has been found to be as follows: H-ZSM-5/50 > H-DeX -15% TFA> HY > H-USY > H-DeX.

The catalytic activity of ZSM-5 series with different $SiO_2/Al_2O_3$ ratio (all in H form) was investigated. The activity of the catalysts decreases with increasing $SiO_2/Al_2O_3$ ratio. H-ZSM-5/50 was found to be a more suitable catalyst for production of light hydrocarbons from aqueous ethanol.

Influences of WHSV, reaction temperature and aqueous ethanol concentration on ethanol dehydration over H-ZSM-5/50 were investigated. It has been found that WHSV and reaction temperature significantly affect the ethanol conversion and the product distribution. The conversion of ethanol and the yield of ethylene decrease while WHSV increases. The total conversion nearly reaches 100% after reaction temperature is higher than 225°C, reaction temperature 275°C appears to be the best temperature for the production of ethylene plus propylene. With increasing aqueous ethanol concentration the conversion increases, but the ethylene selectivity only changes a little.

# References


1. W. R. Moser, C. C. Chiang and R. W. Thompson, J. Catal., 115 (1989) 532
2. R. Le Van Mao and L. H. Dao, U. S. Patent 4608452 (Oct. 6, 1987)
3. R. Le Van Mao, P. Levesque, G. Mclaughlin and L. H. Dao, Appl. Catal., 34 (1987) 163-179
4. R. Le Van Mao, T. M. Nguyen and G. P. Mclaughlin, Appl. Catal., 48 (1989) 265-277
5. A. Corma and J. Perez-Pariente, Clay Miner., 22 (1987) 423-433
6. S. G. Gagarin, R. Z. Zakharyan and Yu. A. Kolbanovskii, Russian Chemical Bulletin, 32 (1983) 1140-1145
7. Winnick, Charles N., *Catalytic process for dehydration of alcohols*, United States Patent 4207424 (1980)
8. Pearson and E. Donald, *Process for catalytic dehydration of ethanol vapour to ethylene*, United States Patent 4423270 (1983-12-27)
9. H.W. Scheeline and R. Itoh, PEP Review 79-3-4, (January 1980)
10. R. Le Van Mao, R. Carli, H. Ahlafi and V. Ragini, Catal. Lett., 6 (1990) 321-330
11. I. Takahara, M. Saito, M. Inaba and K. Murata, Catal. Lett., 105 (2005) 249-257
12. Ben-Zu Wan, S. Cheng, R. G. Anthony and A. Clearfield, J. Chem. Soc., Faraday Trans., 87 (1991) 1419 – 1423
13. S. Kamiguchi and T. Chihara; Catal. Lett., 85 (2003) 97-100
14. J. Haber, K. Pamin, L. Matachowski, B. Napruszewska and J. Poltowicz, J. cataly., 207 (2002) 296-306

15. T. Zaki, J. Colloid Interface Sci., 284 (2005) 606-613

16. T. Zaki and S. Mikhail, Petroleum Science and Technology, 23 (2005) 1479-1497

17. Y. Shinohhara, H. Satozono, T. Nakajima, S. Suzuki and S. Mishima; Journal of Chemical Software, 4 (1997) 41.

18. J. I. Di Cosimo, V. K. Diez, M. Xu, E. Iglesia and C. R. Apesteguia; J. Catal., 178 (1998) 499-510

19. E. G. Derouane, J. B. Nagy, P. Dejaifve, J. H. C. Van Hooff, B. P. Spekman, J. C. Vedrine and C. Naccache, J. Catal., 53 (1978) 40-55

20. C. D. Chang and A. J. Silvestre, J. Catal., 47 (1977) 249-259

21. C. D. Chang, *Hydrocarbons from methanol, Chemical Industries Vol 10*, Marcel Dekker Inc., (1983) p50

22. P. B. Venuto and P. S. Landis, J. Catal., 21 (1971) 330-335

23. R. Arlene, Ph. D. Thesis, Concordia University, (1996)

24. Sami Matar; Lewis F. Hatch, *Chemistry of Petrochemical Processes, 2nd Edition*, Gulf Professional Publishing,Butterworth-Heinemann, (2001,) p205.

25. J. Weitkamp; L. Puppe, *Catalysis and Zeolites Fundaments and Applications*, Springer: Verlag Berlin Heidelberg, (1999) p453

26. Serge Raseev, *Thermal and Catalytic Processes in Petroleum Refining*, Marcel Dekker, Inc. New York and Basel, (2003) p311

27. J. Scherzer, *Octane-Enhancing, Zeolitic FCC Catalysts: Scientific and Technical* Aspects, Marcel Dekker, Inc. New York and Basel, (1990) p91

28. R. H. Grubbs, Tetrahedron, 60 (2004) 7117-7140

29. E. N. Guidry, S. J. Cantrill, J. F. Stoddart, and R. H. Grubbs, Organic Lett., 7(11) (2005) 2129-2132

30. O. A. Scherman, R. Walker, and R. H. Grubbs, Macromolecules, 38 (2005) 9009-9014

31. W. C. P. Tsang, J. A. Jernelius, A. G. Cortez, G. S. Weatherhead, R. R. Schrock, A. H. J. Hoveyda, Am. Chem. Soc., 125 (2003) 2591-2596

32. R. R. Schrock, J. Molec. Catal. A, 213 (2004) 21-30

33. R. R. Schrock, L. P. H. Lopez, J. Hafer, R. Singh, A. Sinha, P. Muller, Organometallics, 24 (2005) 5211-5213

34. Michel Guisnet, Jean-Pierre Gilson, *Zeolite for Cleaner Technologies*, Imperial College Press, London, (2002) p30

35. B. Arstad et al., J. Amer. Chem. Soc., 126 (2004) 2991-3001

36. I. M. Dahl and S. Kolboe, J. Catal., 161 (1996) 304-309

37. I. M. Dahl and S. Kolboe, J. Catal., 149 (1994) 458-464

38. U. Olsbye et al., Catal. Today, 106 (2005) 108-111

39. A. Sassi et al., J. Phys. Chem. B, 106 (2002) 8768-8773

40. M. Seiler et al., Catal. Lett., 88 (2003) 187-191

41. W. Wang, Y. Jiang and M. Hunger, Catal. Lett., 113 (2006) 102-114

42. R. M. Barrer, *Hydrothermal Chemistry of Zeolites*, Academic Pr, (1982)

43. A. Dyer, *An Introduction to Zeolite Molecular Sieves*, John Wiley & Sons, (1988)

44. R. M Barrer, Zeolites, 1 (1981) 130-140

45. W. M. Meier, Pur Appl. Chem., 58 (1986) 1323-1328

46. D. R. Rolison, Chem. Rev., 90 (1990) 867-878

47. J. Weitkamp, Solid State Ionics, 131 (2000) 175-188

48. P. R. Pujado, J. A. Rabo, G. J. Antos and S. A. Gembiki, Catalysis Today, 13 (1992) 113-141

49. R. V. Jasra and S. G. T. Bhai, Sep. Sci. Technol. 23 (1988) 945-989

50. R. Krishna and D. Paschek, Sep. Purif. Technol. 21 (2000) 111-136

51. N. K. Lazaridis, E. N. Peleka, Th. D. Karapanrtsios and K. A. Matis, Hydrometallurgy, 74 (2004) 149-156

52. Z. Go, S. Zheng, Z. Zheng, F. Jiang, W. Hu and L. Ni, Water Research, 39 (2005) 1174-1182

53. A. Coma, Chem. Rev. , 95 (1995) 559-614

54. D. Zhao, Q. Huo, J. Feng, B. F. Chmelka, and G.D. Stucky, J. Am. Chem. Soc., 120 (1998) 6024-6036

55. Jens Hagen, *Industral Catalysis: A Practical approach, Second Edition*, Wiley-VCH Verlag GmbH & Co. KGaA, Weinheim, (2006) p236

56. Q.L. Wang, M. Torrealba, G. Giannetto, M. Guisnet, G. P Caboreau and J. Caisso, Zeolites, 10 (1990 )703-706

57. R. Le Van Mao, N. T. C. Vo, B. Sjiariel, L. Li and Denes, J. Mater. Chem., 2 (1992) 595-599

58. R. Le Van Mao, J. A. Lavigne, B. Sjiariel, J. Mater. Chem., 3 (1993) 679-683

59. R. Le Van Mao, N. T. C. Vo, G. Denes and T. S. Le, J. Porous Mater., 1 (1995) 175-183

60. C. S. Triantafillidis, A. G. Vlessidi, L. Nalbandian and N. P. Evmiridis, Microp. Mesop. Mater., 47 (2001) 369-388

61. N. Y. Chen, C. Morris Smith, Thomas F. Degnan, *Molecular Transport and Reaction in Zeolites: Design and Application of Shape Selective Catalysis*, Wiley & Sons, (1994) p25

62. R. Le Van Mao, S. Xiao, A. Ramsaram and J. Yao, J. Mater. Chem.,4 (1994) 605-610

63. R. Le Van Mao, A. Ramsaram, S. Xiao, J. Yao and V. Semmer, J. Mater. Chem., 5 (1995) 533-535

64. D. Ohayon. R. Le Van Mao, D. Ciaravino, H. Hazel A. Cochennec and N. Rolland, Appl. Catal. A Gen, 217 (2001) 241-251

65. L. Lu, R. Le Van Mao, N. Al-Yassir, A. Muntasar and N. T. Vu, Catal. Lett., 105 (2005) 139-147

66. J. D. de Bore, *The shapes of capillaries, In: The structure and properties of porous materials*, D. H. Everett and F. S. Stone (eds.) London, Butterworths, (1958) p68-94

67. G. Leofanti, M. Padovan, G. Tozzola and B. Venturelii, Catalysis Today, 41 (1998) 207-219

68. R. Le Van Mao, N. Al-Yassir, L. Lu, N. T. Vu and A. Fortier, Catal. Lett., 112 (2006) 13-18

69. Lin Lu, MSc. Thesis, Concordia University, (2005)

70. B. Coasne, A. Grosman, C. Ortaga and M. Simon, Phys. Rev. Lett., 88 (2002) 256102